JCB Journal of Cell Biology

ARTICLE

USP19 promotes hypoxia-induced mitochondrial division via FUNDC1 at ER-mitochondria contact sites

Peiyuan Chai[1], Yiru Cheng[1], Chuyi Hou[1], Lei Yin[2], Donghui Zhang[1], Yingchun Hu[3], Qingzhou Chen[1], Pengli Zheng[1], Junlin Teng[1], and Jianguo Chen[1,4]

The ER tethers tightly to mitochondria and the mitochondrial protein FUNDC1 recruits Drp1 to ER-mitochondria contact sites, subsequently facilitating mitochondrial fission and preventing mitochondria from undergoing hypoxic stress. However, the mechanisms by which the ER modulates hypoxia-induced mitochondrial fission are poorly understood. Here, we show that USP19, an ER-resident deubiquitinase, accumulates at ER-mitochondria contact sites under hypoxia and promotes hypoxia-induced mitochondrial division. In response to hypoxia, USP19 binds to and deubiquitinates FUNDC1 at ER-mitochondria contact sites, which facilitates Drp1 oligomerization and Drp1 GTP-binding and hydrolysis activities, thereby promoting mitochondrial division. Our findings reveal a unique hypoxia response pathway mediated by an ER protein that regulates mitochondrial dynamics.

Introduction

Mitochondria are dynamic organelles shaped continuously by fission and fusion to regulate their function in response to cellular stress, and defects in mitochondrial dynamics cause multiple severe human diseases, such as neurodegenerative disorders and muscle atrophy (Chan, 2012; Chen and Chan, 2017; Mishra and Chan, 2014; Romanello et al., 2010; Youle and van der Bliek, 2012). Dynamin-related protein 1 (Drp1) is the master regulator of mitochondrial fission (Smirnova et al., 1998). During mitochondrial fission, once recruited to fission sites by Drp1 receptors, such as Mff (Gandre-Babbe and van der Bliek, 2008; Otera et al., 2010), Fis1 (Yoon et al., 2003), MiD49, and MiD51 (Losón et al., 2013), Drp1 oligomerizes into a helical ring around the fission sites and constricts the mitochondrion in a GTP-dependent manner (Ingerman et al., 2005).

The ER has been shown to participate in Drp1-mediated mitochondrial division (Friedman et al., 2011; Korobova et al., 2013). ER tubules wrap around the mitochondria and determine the fission sites. Drp1 is recruited to these ER-mitochondrial contacts to complete mitochondrial fission (Friedman et al., 2011). Actin filaments induced by ER-localized formin 2 drive initial mitochondrial constriction by directly binding to Drp1 and promoting Drp1 oligomerization (Hatch et al., 2016; Ji et al., 2015; Korobova et al., 2013). As the Drp1 receptors Mff and Fis1 localize to the ER, the ER acts as a new platform for Drp1 oligomerization (Ji et al., 2017). Drp1 transfers from the ER to mitochondria, mediating mitochondrial division (Ji et al., 2017).

The ER contacts the mitochondria and creates a membrane domain that functions as a platform in response to stimuli (Hamasaki et al., 2013; Wu et al., 2016; Zheng et al., 2018). As a critical stressor under physiological and pathological conditions, hypoxia induces closer ER-mitochondria tethering, leading to mitochondrial fission and mitophagy (Kim et al., 2011; Liu et al., 2012; Wu et al., 2016). In response to hypoxia, FUNDC1, a mitochondrial outer membrane protein, accumulates at the ER-mitochondria contact sites, recruiting Drp1 to ensure hypoxia-induced mitochondrial fission (Wu et al., 2016), and subsequently interacts with LC3 to complete mitophagy (Liu et al., 2012); however, the role of the ER in hypoxia-induced mitochondrial division remains poorly understood. Moreover, FUNDC1 is precisely regulated in hypoxic cells (Chen et al., 2017; Liu et al., 2012). Following hypoxia stimulation, FUNDC1 is dephosphorylated, which triggers activation of mitophagy (Liu et al., 2012), and then is ubiquitinated by MARCH5 (also called MITOL) and degraded in a proteasomal-dependent manner (Chen et al., 2017). The deubiquitinase of FUNDC1, however, remains unknown.

Ubiquitin-specific protease 19 (USP19) was first identified as a deubiquitinase that is upregulated in skeletal muscle atrophying during catabolic states (Combaret et al., 2005). USP19

[1]Key Laboratory of Cell Proliferation and Differentiation of the Ministry of Education and State Key Laboratory of Membrane Biology, College of Life Sciences, Peking University, Beijing, China; [2]State Key Laboratory of Protein and Plant Genetic Engineering, College of Life Sciences, Peking University, Beijing, China; [3]Core Facilities, College of Life Sciences, Peking University, Beijing, China; [4]Center for Quantitative Biology, Peking University, Beijing, China.

Correspondence to Jianguo Chen: chenjg@pku.edu.cn; Junlin Teng: junlinteng@pku.edu.cn.

was subsequently shown to localize to the ER and participate in ER-associated degradation (Hassink et al., 2009), the hypoxia pathway (Altun et al., 2012), apoptosis (Mei et al., 2011), autophagy (Jin et al., 2016), the innate immune pathway (Jin et al., 2016), and unconventional protein secretion processes (Lee et al., 2016). In the present study, we show that USP19 promotes hypoxia-induced mitochondrial fission. USP19 is a mitochondria-associated ER membrane (MAM) protein that accumulates at ER-mitochondria contact sites under hypoxia. In response to hypoxia, USP19 tends to interact with FUNDC1, removing the ubiquitin chains from FUNDC1 at MAM and stabilizing FUNDC1 at ER-mitochondria contact sites, thereby facilitating the oligomerization of Drp1 at the ER-mitochondria contact sites to complete the fission events. Our findings describe a critical role for the ER in mitochondrial dynamics in response to hypoxia.

Results

USP19 promotes hypoxia-induced mitochondrial fission

USP19, an ER-resident deubiquitinase (Hassink et al., 2009), stabilizes hypoxia-inducible factor 1α (HIF1α) under hypoxia (Altun et al., 2012). To reveal the function of USP19 on hypoxia-induced pathways, such as mitochondrial fragmentation (Kim et al., 2011; Liu et al., 2012), we first generated USP19 knockout (KO) HeLa cells (Fig. S1, A and B) using a CRISPR/Cas9 approach (Ran et al., 2013). Subsequently, we determined the hypoxia induction efficacy by measuring the expression of HIF1α (Fig. S1 C; Kenneth and Rocha, 2008) and observed that the percentage of WT cells containing fragmented mitochondria increased dramatically 4 h after exposure to hypoxia (1% O_2), with greater than 80% of cells exhibiting fragmented mitochondria at 16 h after exposure (Fig. S1, D and E). Surprisingly, we found only 26% of cells containing fragmented mitochondria in a USP19-deficient background 16 h after exposure to hypoxia (Fig. 1, A and B; and Fig. S1 F), whereas USP19 deficiency did not result in any significant change in mitochondrial morphology under normoxia (Fig. 1, A and B). Overexpression of WT USP19, but not catalytically inactive (C506S; Hassink et al., 2009) or transmembrane domain deletion (USP19ΔTMD, residues 1–1,291) mutants (Fig. S1 G), rescued the change in mitochondrial morphology displayed by USP19 KO cells under hypoxia (Fig. 1, A and B), indicating that the deubiquitinase activity and ER localization of USP19 are required for its function. Consistently, EM analysis confirmed that depletion of USP19 in hypoxic cells significantly inhibited mitochondrial fragmentation (Fig. 1 C). Furthermore, the role of USP19 in hypoxia-induced mitochondrial dynamics was verified to be specific, since hypoxic USP19 KO cells did not exhibit any obvious changes in the ER or peroxisomes (Fig. S2, A–C).

We next asked whether USP19 affects the balance between mitochondrial fusion and fission under hypoxia. To examine mitochondrial fusion activity, we adopted a photoactivation technique where cell-expressed mitochondrial matrix–targeted photoactivatable GFP (mito-PAGFP) is activated in a region of interest (ROI), followed by fluorescence decay, and the dilution rate is proportional to the number of fusion events (Karbowski et al., 2004). Live cell images revealed that USP19 deficiency did not cause any obvious changes in the dilution rate in hypoxic cells (Fig. S2, D and E). We subsequently labeled mitochondria with MitoTracker Red to determine whether USP19 contributes to hypoxia-induced mitochondrial fission. USP19 KO cells exhibited decreased fission rates under hypoxia (Fig. 1, D and E), suggesting that USP19 functions in mitochondrial fission under hypoxia. Taken together, these results indicate that USP19 promotes hypoxia-induced mitochondrial division.

USP19 is a MAM protein that accumulates in the MAM in response to hypoxia

To investigate how USP19 regulates hypoxia-induced mitochondrial division, we examined whether USP19 localizes at ER-mitochondria contact sites, which is vital for mitochondrial dynamics (Friedman et al., 2011). We analyzed the subcellular distribution of USP19 by Percoll density-gradient centrifugation (Frezza et al., 2007; Wieckowski et al., 2009) in mouse skeletal muscle, which highly expresses USP19 (Combaret et al., 2005), and found that USP19 was present in the MAM fraction (Fig. 2 A) along with the well-established MAM protein long-chain fatty acid-CoA ligase 4 (FACL4) and several other MAM-localized proteins, such as calnexin, voltage-dependent anion channel 2 (VDAC2), and mitofusin 2 (MFN2; de Brito and Scorrano, 2008; Wieckowski et al., 2009). This result suggests that USP19 is a MAM protein.

We next assessed whether the level of USP19 in the MAM changes in response to hypoxia using Percoll density-gradient centrifugation in HeLa cells. Consistent with previous reports (Liu et al., 2012; Wu et al., 2016), FUNDC1 that was present in the pure mitochondrial fraction decreased in response to hypoxia (Fig. 2 B and Fig. S3 A), while FUNDC1, FACL4, and Drp1 present in the MAM fraction significantly increased (Fig. 2 B and Fig. S3, B–D). Neither USP30, a mitochondrial outer membrane deubiquitinase (Fig. 2 B and Fig. S3 E), nor the ER protein calnexin (CNX; Fig. 2 B and Fig. S3 F) was changed in the MAM fraction under hypoxia. Importantly, USP19 was markedly accumulated in the MAM fraction in response to hypoxia (Fig. 2, B and C); however, the level of ER-localized USP19 remained unchanged (Fig. 2, B and D).

To further confirm the hypoxia-induced USP19 accumulation at ER-mitochondria contact sites, we examined its cellular localization. Since a USP19 antibody for immunofluorescence was not available, we developed 3×Flag-mNeonGreen-USP19 knock-in HeLa cells (Fig. S3, G and H) and found that endogenous mNeonGreen-USP19 was significantly accumulated around mitochondria and partially colocalized with mitochondria marked by TOM20 under hypoxia (Fig. 2 E). We also performed a proximity ligation assay (PLA) by probing for VDAC1, a MAM protein that does not accumulate at ER-mitochondria contact sites under hypoxia (Fig. 2 B; Wu et al., 2016), and endogenous USP19 in these knock-in cells. Compared with cells under normoxia, the number of red PLA-positive puncta representing VDAC1 sites associated with USP19 was significantly increased in hypoxic cells (Fig. 2, F and G), illustrating that USP19 accumulates at ER-mitochondria contact sites in response to hypoxia. Immuno-EM further verified the accumulation of USP19 at the ER-mitochondria contact sites in knock-in cells under hypoxia (Fig. 2, H and I). Moreover, USP19 did not affect ER tethering to

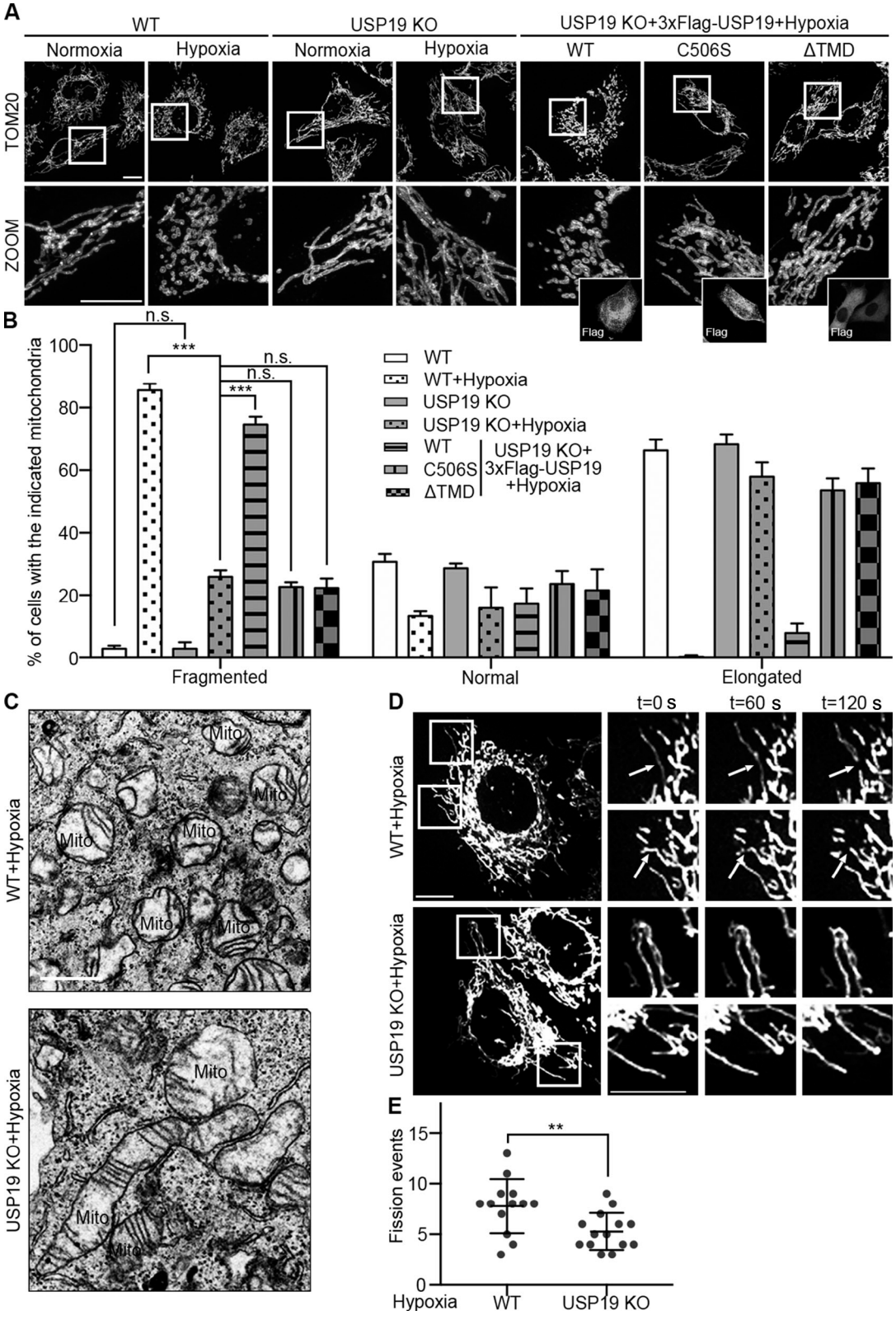

Figure 1. **USP19 promotes hypoxia-induced mitochondrial fission. (A)** Representative confocal images of mitochondrial morphology in WT and USP19 KO HeLa cells under hypoxia. WT, USP19 KO, or USP19 KO cells transfected with 3×Flag-USP19 WT, 3×USP19 catalytically inactive mutant (C506S), or 3×USP19 transmembrane domain (TMD) deletion mutant (ΔTMD, residues 1–1,291) were exposed to normoxia or hypoxia for 16 h, followed by coimmunostained for Flag and TOM20. An enlargement of the hatched box is shown. Scale bar, 10 µm. **(B)** Quantification of mitochondrial morphology in A. The bars represent mean ± SEM. ***, P < 0.001, unpaired two-tailed Student's *t* test, three independent experiments, *n* ≥ 300 cells. **(C)** Representative EM images of mitochondrial morphology in WT and USP19 KO HeLa cells exposed to normoxia or hypoxia for 8 h. Scale bar, 1 µm. Mito, mitochondria. **(D)** Live cell images of WT and USP19

KO HeLa cells exposed to hypoxia for 8 h and stained with MitoTracker Red. Arrows indicate mitochondrial fission events. Scale bar, 10 µm. **(E)** Number of mitochondrial fission events in D counted over a 7.5-min period. Bars represent mean ± SEM. **, P < 0.01, unpaired two-tailed Student's *t* test, three independent experiments, *n* ≥ 13 cells.

mitochondria under hypoxia as shown by a PLA probed for the mitochondrial protein TOM20 and the ER protein calnexin (Fig. S3, I and J).

USP19 interacts with FUNDC1 and promotes FUNDC1 localization to the MAM under hypoxia

Accumulation of FUNDC1 in the MAM (Fig. 2 B and Fig. S3 B) and subsequent facilitation of the recruitment of Drp1 to the MAM are required for hypoxia-induced mitochondrial division (Wu et al., 2016). We next examined whether USP19 interacts with FUNDC1. Immunoprecipitation assays in HEK293T cells revealed that exogenously expressed USP19 interacted strongly with FUNDC1 (Fig. 3 A), but hardly with Drp1 receptors, such as Mff, Fis1, MiD49, and MiD51 (Fig. S4 A). Hypoxia enhanced the interaction of endogenous USP19 with FUNDC1, but not with MFN2 (Fig. 3 B), a mitochondrial outer membrane protein vital

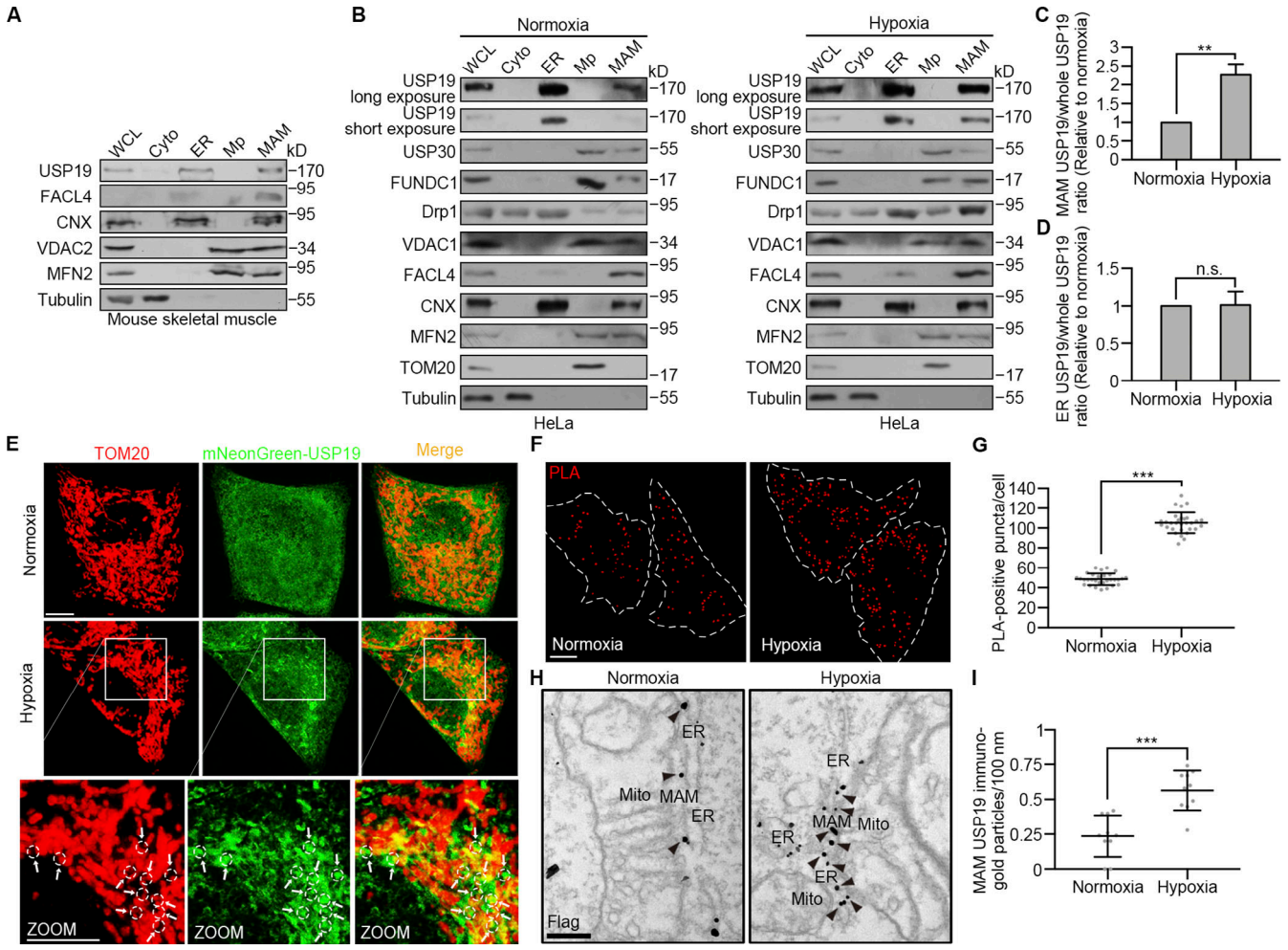

Figure 2. **USP19 is a MAM protein that accumulates in the MAM under hypoxia. (A)** Western blot analysis of subcellular fractions from mouse skeletal muscle. Cyto, cytosol; Mp, pure mitochondria; WCL, whole-cell lysate. **(B)** Western blot analysis of subcellular fractions from HeLa cells exposed to normoxia or hypoxia for 8 h. **(C)** Quantification of the ratio of USP19 in the MAM in B. Bar represents mean ± SEM. **, P < 0.01, unpaired two-tailed Student's *t* test, three independent experiments. **(D)** Quantification of the ratio of ER USP19 in B. Bar represents mean ± SEM; unpaired two-tailed Student's *t* test, three independent experiments. **(E)** Representative images of 3×Flag-mNeonGreen-USP19 knock-in HeLa cells exposed to normoxia or hypoxia for 8 h. Cells were immunostained for TOM20 (red). Arrows indicate endogenous mNeonGreen-USP19 (green) accumulation around mitochondria (red). Scale bar, 10 µm. **(F)** 3×Flag-mNeonGreen-USP19 knock-in HeLa cells exposed to normoxia or hypoxia for 8 h were subjected to PLA with anti-VDAC1 and anti-Flag antibodies. Projections of z-stacked representative images are shown. Scale bar, 10 nm. **(G)** Quantification of the number of PLA-positive puncta/cell in F. Bars represent mean ± SEM. ***, P < 0.001, unpaired two-tailed Student's *t* test, three independent experiments, *n* ≥ 30 cells. **(H)** Immuno-gold labeling of resin sections with an anti-Flag antibody in 3×Flag-mNeonGreen-USP19 knock-in HeLa cells exposed to normoxia or hypoxia for 8 h. Arrowheads indicate gold particle–labeled endogenous 3×Flag-mNeonGreen-USP19 in the MAM. Scale bar, 200 nm. **(I)** Quantification of the MAM USP19-labeled gold particles per 100 nm MAM length in H. Bars represent mean ± SEM. ***, P < 0.001, unpaired two-tailed Student's *t* test, three independent experiments, *n* ≥ 10 MAMs.

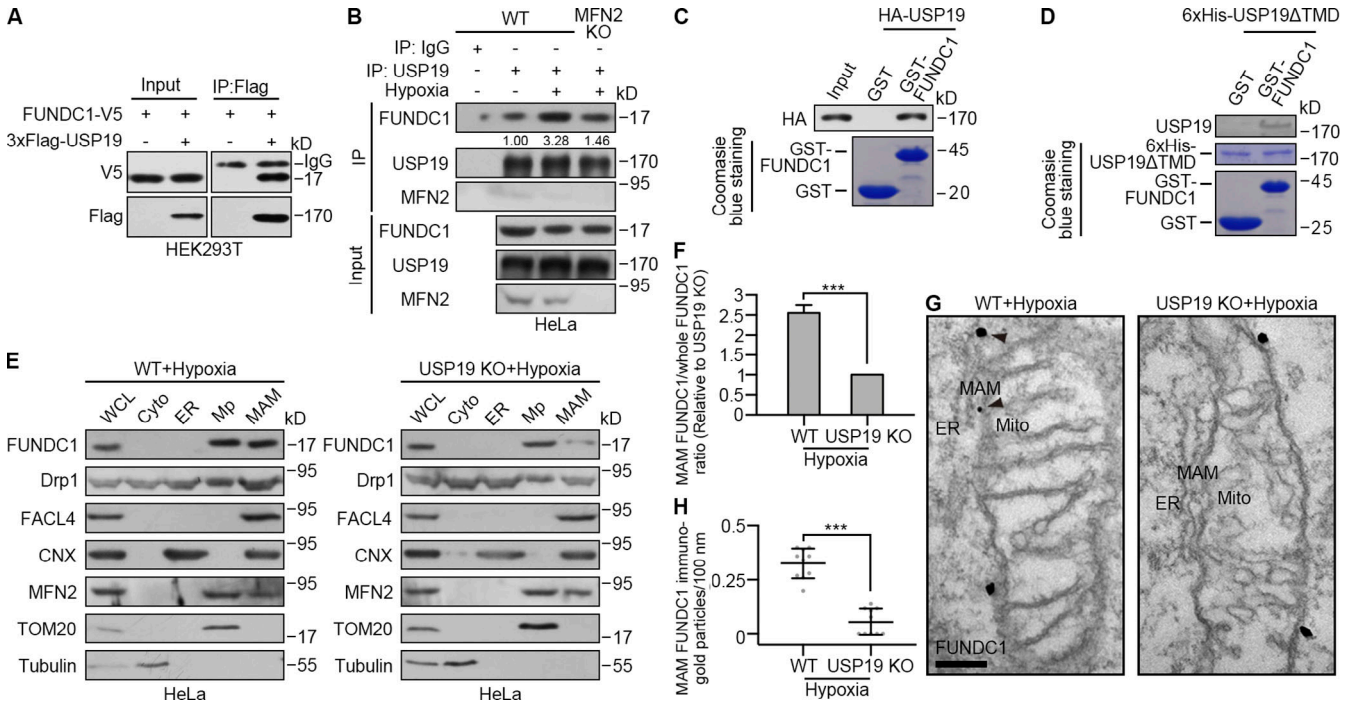

Figure 3. **USP19 interacts with and promotes FUNDC1 accumulation in the MAM under hypoxia. (A)** Lysates from HEK293T cells cotransfected with 3×Flag-USP19 and FUNDC1-V5 were immunoprecipitated (IP) with an anti-Flag antibody. Immunoprecipitated samples were analyzed by Western blotting. **(B)** Lysates from WT and MFN2 KO HeLa cells exposed to normoxia or hypoxia for 8 h were immunoprecipitated with an anti-USP19 antibody and IgG (negative control). Immunoprecipitated samples were analyzed using Western blotting. Relative ratio of FUNDC1 to USP19 was quantified and normalized to cells under normoxia. **(C)** Lysates from HEK293T cells expressing HA-USP19 were incubated with glutathione Sepharose 4B beads conjugated to GST or GST-FUNDC1. Samples were analyzed using Western blotting with the indicated antibodies and Coomassie blue staining. **(D)** GST or GST-FUNDC1, expressed in BL21 cells, were prepurified with glutathione Sepharose 4B beads and incubated with purified 6×His-USP19ΔTMD (cytosolic domain of USP19, residues 1–1,291) from BL21 cells, and samples were analyzed using Western blotting with an anti-USP19 antibody and Coomassie blue staining. **(E)** Western blot analysis of subcellular fractions from WT and USP19 KO HeLa cells exposed to hypoxia for 8 h. Cyto, cytosol; Mp, pure mitochondria; WCL, whole-cell lysate. **(F)** Quantification of the ratio of FUNDC1 in the MAM in E. Bar represents mean ± SEM. ***, P < 0.001, unpaired two-tailed Student's *t* test, three independent experiments. **(G)** Immuno-gold labeling of resin sections with an anti-FUNDC1 antibody in WT and USP19 KO HeLa cells exposed to hypoxia for 8 h. Arrowheads indicate gold particle–labeled endogenous FUNDC1 in the MAM. Mito, mitochondria. Scale bar, 200 nm. **(H)** Quantification of the MAM FUNDC1 gold particles per 100 nm MAM length in G. Bars represent mean ± SEM. ***, P < 0.001, unpaired two-tailed Student's *t* test, three independent experiments, $n \geq 10$ MAMs.

for MAM formation (de Brito and Scorrano, 2008; Sugiura et al., 2013). Furthermore, GST pull-down assays using immunoprecipitated HA-USP19 from HEK293T cells and purified GST-tagged FUNDC1 from *BL21* cells verified the interaction of USP19 with FUNDC1 (Fig. 3 C). We also purified GST-tagged FUNDC1 and the His-tagged cytosolic domain of USP19 (6×His-USP19ΔTMD, residues 1–1,291) from *BL21* cells to perform in vitro pull-down assays. GST-FUNDC1 bound to 6×His-USP19ΔTMD (Fig. 3 D), suggesting that USP19 binds directly to FUNDC1. Moreover, the interaction of USP19 with FUNDC1 was weakened in hypoxic MFN2 KO HeLa cells compared with that in hypoxic WT HeLa cells (Fig. 3 B and Fig. S4, B and C), suggesting that the association between USP19 and FUNDC1 under hypoxia is dependent on MAM formation.

We next examined whether USP19 affects the MAM localization of FUNDC1 under hypoxia. Interestingly, FUNDC1 was barely detected in the MAM fraction from USP19 KO HeLa cells under hypoxia (Fig. 3, E and F). Immuno-EM further showed that USP19 deficiency prevented hypoxia-induced accumulation of endogenous FUNDC1 at ER-mitochondria contact sites (Fig. 3, G and H). These results indicate that USP19 is required for FUNDC1 accumulation in the MAM under hypoxia.

USP19 deubiquitinates FUNDC1 at K119 in the MAM under hypoxia

Since USP19 is a deubiquitinase (Combaret et al., 2005), we evaluated whether USP19 deubiquitinates FUNDC1. WT USP19, but not the catalytically inactive C506S mutant, decreased ubiquitination of FUNDC1 in HEK293T cells (Fig. 4 A). In vitro deubiquitination assays using immunopurified USP19 and ubiquitinated FUNDC1 from HEK293T cells further confirmed that WT USP19 directly deconjugated ubiquitin chains from FUNDC1, but the catalytically inactive USP19 mutant did not (Fig. 4 B). We next wondered whether USP19 affects the ubiquitination level of FUNDC1 in the MAM. As a FUNDC1 antibody could not be used to perform immunoprecipitation assays, we established FUNDC1 KO and USP19/FUNDC1 double KO (DKO) HeLa cells that stably expressed FUNDC1-Flag in which the protein expression level of FUNDC1-Flag was comparable with that of endogenous FUNDC1 (Fig. S4, D and E; FUNDC1 KO-FUNDC1-Flag, USP19/FUNDC1 DKO-FUNDC1-Flag). The

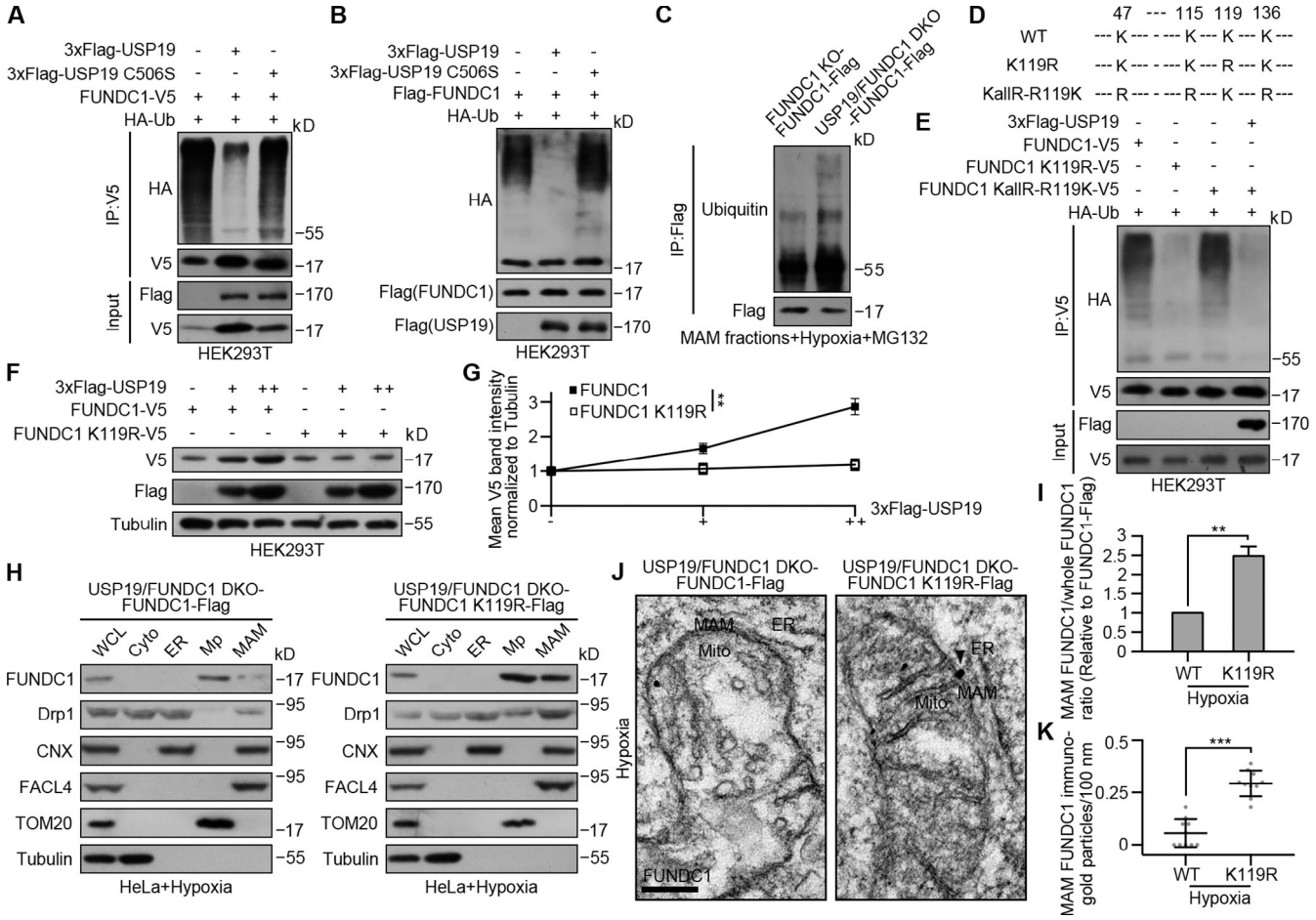

Figure 4. **USP19 deubiquitinates FUNDC1 at lysine 119 in the MAM under hypoxia. (A)** Lysates from HEK293T cells cotransfected with the indicated plasmids were immunoprecipitated (IP) with an anti-V5 antibody. Immunoprecipitated samples were analyzed using Western blotting. **(B)** Purified ubiquitinated FUNDC1 from HEK293T cells was incubated with immunopurified 3×Flag-USP19 from HEK293T cells in vitro, and samples were analyzed by Western blotting with anti-HA and anti-Flag antibodies. **(C)** Immunoprecipitated endogenous ubiquitin in the MAM fractions derived from hypoxic FUNDC1 KO and USP19/FUNDC1 DKO HeLa cells stably expressing FUNDC1-Flag (FUNDC1 KO-FUNDC1-Flag, USP19/FUNDC1 DKO-FUNDC1-Flag) were treated with MG132 (10 μM), a proteasome inhibitor, for 8 h. Immunoprecipitated samples were analyzed using Western blotting. **(D)** Schematic of the FUNDC1 mutants. K119R, the lysine (K) 119 to arginine (R); KallR-R119K, all the K except K119 to R. **(E)** Lysates from HEK293T cells cotransfected with the indicated plasmids were immunoprecipitated with an anti-V5 antibody. Immunoprecipitated samples were analyzed using Western blotting. **(F)** Western blot analysis of lysates from HEK293T cells cotransfected with 3×Flag-USP19 and FUNDC1-V5 or FUNDC1 K119R-V5. +, low expression; ++, high expression. Tubulin served as a loading control. **(G)** Densitometric mean band intensity of the Western blots in F. Bars represent mean ± SEM. **, $P < 0.01$, unpaired two-tailed Student's *t* test, three independent experiments. **(H)** Western blot analysis of subcellular fractions from USP19/FUNDC1 DKO HeLa cells stably expressing FUNDC1-Flag (USP19/FUNDC1 DKO-FUNDC1-Flag) or FUNDC1 K119R-Flag (USP19/FUNDC1 DKO-FUNDC1 K119R-Flag) were exposed to hypoxia for 8 h. Cyto, cytosol; Mp, pure mitochondria; WCL, whole-cell lysate. **(I)** Quantification of the ratio of Flag-tagged FUNDC1 in the MAM in H. Bar represents mean ± SEM. **, $P < 0.01$, unpaired two-tailed Student's *t* test, three independent experiments. **(J)** Immuno-gold labeling of resin sections with an anti-FUNDC1 antibody in USP19/FUNDC1 DKO-FUNDC1-Flag and USP19/FUNDC1 DKO FUNDC1 K119R-Flag cells exposed to hypoxia for 8 h. Arrowhead indicates gold particle–labeled FUNDC1 in the MAM. Mito, mitochondria. Scale bar, 200 nm. **(K)** Quantification of the MAM FUNDC1 gold particles per 100 nm MAM length in J. Bars represent mean ± SEM. ***, $P < 0.001$, unpaired two-tailed Student's *t* test, three independent experiments, $n \geq 10$ MAMs.

ubiquitination of FUNDC1 was significantly increased in the MAM fraction of hypoxic USP19/FUNDC1 DKO-FUNDC1-Flag cells compared with that of hypoxic FUNDC1 KO-FUNDC1-Flag cells (Fig. 4 C), suggesting that USP19 is required for deubiquitination of FUNDC1 at the MAM under hypoxia.

We subsequently determined the FUNDC1 sites that are deubiquitinated by USP19. Since FUNDC1 is reported to be ubiquitinated at lysine 119 by MARCH5 under hypoxia (Chen et al., 2017), we generated two FUNDC1 mutants, lysine (K) 119 to arginine (R; K119R) and all K except K119 to R (KallR-R119K; Fig. 4 D). Consistent with the previous study (Chen et al., 2017), we observed that FUNDC1 K119R displayed a lower ubiquitination level than that of WT FUNDC1, whereas no significant reduction was seen in the ubiquitination level of FUNDC1 KallR-R119K (Fig. 4 E). USP19 overexpression reduced the ubiquitination of FUNDC1 (Fig. 4 E). Moreover, the level of USP19 was positively correlated with the level of WT FUNDC1, but not with the levels of the K119R mutant, Mff, Fis1, MiD49, or MiD51 (Fig. 4, F and G; and Fig. S4 F).

To determine whether MAM-localized FUNDC1 stability is regulated by USP19 under hypoxia, we performed subcellular fraction assays with FUNDC1 KO and USP19/FUNDC1 DKO HeLa

cells stably expressing FUNDC1-Flag or FUNDC1 K119R-Flag. We found that FUNDC1 K119R had increased accumulation at the MAM in a USP19-deficient background in response to hypoxia (Fig. 4, H and I), while this accumulation could be barely detected in a WT USP19 background (Fig. S4, G and H). Immune-EM confirmed that hypoxia-induced FUNDC1 K119R was more abundant at ER-mitochondria contact sites than WT FUNDC1 in USP19 KO cells (Fig. 4, J and K). Collectively, these data suggest that USP19 stabilizes MAM-localized FUNDC1 through deubiquitination of FUNDC1 at K119 under hypoxia.

USP19-mediated FUNDC1 deubiquitination facilitates hypoxia-induced Drp1 oligomerization and GTPase activity

Once recruited to mitochondrial fission sites determined by the ER (Friedman et al., 2011), Drp1 oligomerizes into a helical ring around the fission sites and constricts the mitochondrion in a GTP-dependent manner (Ingerman et al., 2005). We assumed that USP19-mediated FUNDC1 stabilization stimulates Drp1 oligomerization and is necessary for hypoxia-induced mitochondrial fragmentation. To test this possibility, we first performed sucrose density gradient centrifugation of the crude mitochondrial fraction and found that Drp1 oligomerization was attenuated in hypoxic USP19/FUNDC1 DKO compared with WT cells (Fig. 5, A and B). This attenuation of USP19/FUNDC1 DKO could be rescued by stably overexpressing FUNDC1 K119R, but not WT FUNDC1 (Fig. 5, A and B), suggesting that USP19 promotes Drp1 oligomerization at mitochondria in a FUNDC1 K119–dependent manner. We next examined the effect of FUNDC1 stabilization by USP19 on the GTP binding and hydrolysis abilities of Drp1 (Sugiura et al., 2013). We incubated the lysates of mitochondrial fractions from hypoxic HeLa cells with GTP-agarose. Compared with WT, USP19/FUNDC1 DKO inhibited GTP binding of Drp1 on mitochondria (Fig. 5, C and D). As expected, the reduction in Drp1 GTP binding ability in hypoxic USP19/FUNDC1 DKO cells could be restored by overexpressing the FUNDC1 K119R mutant, but not WT FUNDC1 (Fig. 5, C and D). Consistently, GTP hydrolysis of Drp1 was inhibited in hypoxic USP19/FUNDC1 DKO HeLa cells compared with hypoxic WT cells in the crude mitochondrial fraction, as shown by fluorograms of TLC (Fig. 5, E and F). The decreased GTP hydrolysis abilities of Drp1 remained unchanged in USP19/FUNDC1 DKO-FUNDC1-Flag cells but increased to normal levels in USP19/FUNDC1 DKO-FUNDC1 K119R-Flag cells under hypoxia (Fig. 5, E and F). As a control, in Drp1 KO HeLa cells, we overexpressed a mutant of Drp1 (R403C) identified in children with epileptic encephalopathy that impairs its oligomerization but allows for dimer formation (Fahrner et al., 2016), and we detected a dramatic decrease in both GTP binding and hydrolysis abilities of Drp1 compared with those of Drp1 KO cells expressing WT Drp1 (Fig. S5, A–D), indicating that the immunoprecipitated Drp1 examined here is still oligomeric.

Finally, we examined whether USP19 affects the function of Drp1 on mitochondrial fission in hypoxic cells through FUNDC1. After exposure to hypoxia for 16 h, abundant mitochondria-associated Drp1 puncta, which represent oligomeric Drp1 (Ji et al., 2017), and fragmented mitochondria were observed in hypoxic WT cells, whereas in hypoxic USP19/FUNDC1 DKO cells, few Drp1 puncta were detected on mitochondria and the mitochondria remained elongated (Fig. 5, G–I). Stable overexpressing FUNDC1 K119R-Flag, but not WT FUNDC1-Flag, in these DKO cells rescued the phenotype (Fig. 5, G–I). These results indicate that FUNDC1 K119, regulated by USP19, is crucial for the hypoxia-induced increase in Drp1 oligomerization at mitochondria and mitochondrial fragmentation.

Taken together, these data suggest that USP19 stabilizes FUNDC1, thereby promoting Drp1 oligomerization at ER-mitochondria contact sites in response to hypoxia and resulting in mitochondrial fragmentation.

Discussion

Our study shows that USP19, an ER-resident deubiquitinase, is an MAM protein that accumulates at ER-mitochondria contact sites in response to hypoxia, allowing for its strong interaction with FUNDC1 and deconjugation of its ubiquitin chains. Stabilization of FUNDC1 at the ER-mitochondria contact sites by USP19 is necessary for Drp1 oligomerization and GTPase activity, which facilitates hypoxia-induced mitochondrial fission (Fig. 6). Our findings expand the role of ER proteins in mitochondrial dynamics in response to specific stimuli.

Under normoxia, USP19 does not affect mitochondrial morphology (Fig. 1, A and B). This observation may be explained by the small amounts of FUNDC1 (Wu et al., 2016) and USP19 at the ER-mitochondria contact sites under these conditions (Fig. 2 B), resulting in minimal interaction between these two proteins. In response to hypoxia, both FUNDC1 and USP19 accumulate at ER-mitochondria contact sites, allowing for their strong interaction, which is required for hypoxia-induced mitochondrial division. Calnexin is reported to recruit FUNDC1 to ER-mitochondria contact sites at the early stage of hypoxia (Wu et al., 2016). Whether calnexin recruits USP19 to ER-mitochondria contact sites and the mechanisms of USP19 accumulation in response to hypoxia remain to be uncovered. Interestingly, USP19 also interacts with Drp1 (Fig. S5, E and F), although the protein level of Drp1 is not regulated by USP19 (Fig. S5 G). Since the ER also serves as a platform for Drp1 oligomerization (Ji et al., 2017), USP19 may possibly function as an ER-resident deubiquitinase that regulates Drp1 in a proteasomal-independent manner—for instance, by deconjugating K63-linked polyubiquitin chains from Drp1 that are involved in the regulation of protein localization and activation (Komander and Rape, 2012), subsequently regulating ER-associated oligomeric Drp1 transfer to ER-mitochondria contact sites, which requires further investigation. Given that FUNDC1 binds to both Drp1 (Wu et al., 2016) and USP19 (Fig. 3, A–D), it is plausible that USP19, FUNDC1, and Drp1 function in concert at the ER-mitochondria contact sites as a complex that mediates hypoxia-induced mitochondrial fission.

Actin filaments bind directly to Drp1 and stimulate Drp1 GTPase activity (Ji et al., 2015). ER-localized inverted formin 2, which facilitates actin polymerization, is reported to be required for Drp1-mediated mitochondrial division (Korobova et al., 2013), whereas cofilin1, which promotes actin depolymerization, has been identified as a negative regulator of Drp1-mediated mitochondrial division (Rehklau et al., 2017).

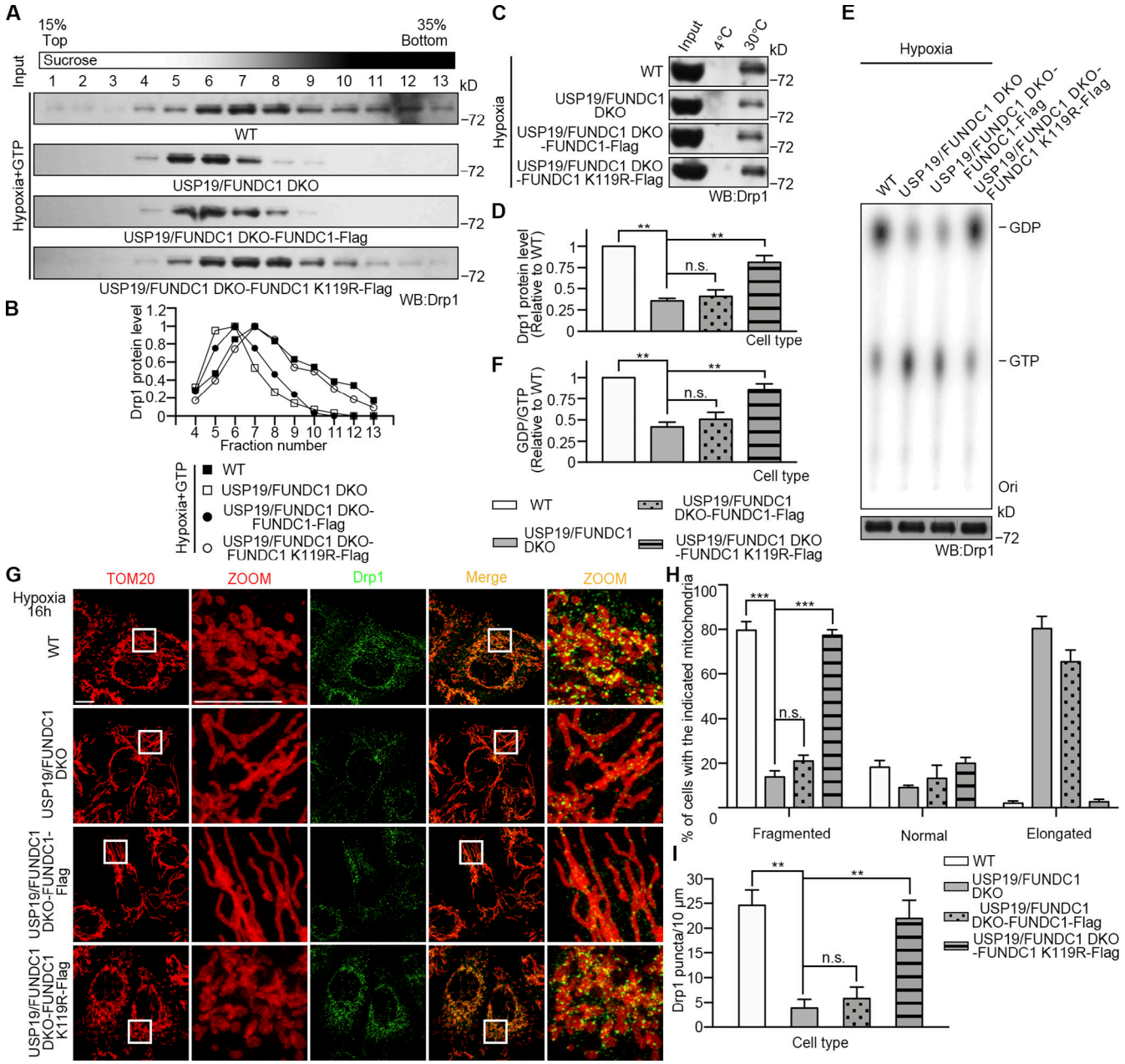

Figure 5. **USP19 promotes oligomerization and GTPase activity of Drp1 in the MAM in response to hypoxia. (A)** Crude mitochondrial fractions derived from WT, USP19/FUNDC1 DKO, and USP19/FUNDC1 DKO HeLa cells stably expressing FUNDC1-Flag (USP19/FUNDC1 DKO-FUNDC1-Flag) or FUNDC1 K119R-Flag (USP19/FUNDC1 DKO-FUNDC1 K119R-Flag) were exposed to hypoxia for 8 h and analyzed for Drp1 oligomerization by sucrose density gradient centrifugation assays. Samples were analyzed by Western blotting (WB) with an anti-Drp1 antibody. **(B)** Quantification of high-molecular-weight Drp1 in A. Three independent experiments. **(C)** Lysates of mitochondrial fractions derived from WT, USP19/FUNDC1 DKO, USP19/FUNDC1 DKO-FUNDC1-Flag, and USP19/FUNDC1 DKO-FUNDC1 K119R-Flag HeLa cells were exposed to hypoxia for 8 h and incubated with GTP-agarose beads. Samples were analyzed by Western blotting with an anti-Drp1 antibody. **(D)** Quantification of GTP binding Drp1 in C. Bars represent mean ± SEM. **, $P < 0.01$, unpaired two-tailed Student's *t* test, three independent experiments. **(E)** Lysates of mitochondrial fractions derived from WT, USP19/FUNDC1 DKO, USP19/FUNDC1 DKO-FUNDC1-Flag, and USP19/FUNDC1 DKO-FUNDC1 K119R-Flag HeLa cells were exposed to hypoxia for 8 h and immunoprecipitated with an anti-Drp1 antibody. Immunopurified endogenous Drp1 was incubated with [α-32P] GTP and analyzed by TLC. Western blot analysis of Drp1 served as loading control. **(F)** Quantification of the ratio of GDP to GTP in E. Bars represent mean ± SEM. **, $P < 0.01$, unpaired two-tailed Student's *t* test, three independent experiments. **(G)** Representative confocal images of mitochondria (red) and Drp1 puncta (green). WT, USP19/FUNDC1 DKO, USP19/FUNDC1 DKO-FUNDC1-Flag, and USP19/FUNDC1 DKO-FUNDC1 K119R-Flag cells were exposed to hypoxia for 16 h and coimmunostained for TOM20 (red) and Drp1 (green). An enlargement of the hatched box is shown on the right of the panels. Scale bar, 10 μm. **(H and I)** Quantification of mitochondrial morphology and Drp1 puncta per mitochondrial length in G. Bars represent mean ± SEM. **, $P < 0.01$; ***, $P < 0.001$, unpaired two-tailed Student's *t* test, three independent experiments, $n \geq 300$ cells in B; $n \geq 30$ mitochondria in G.

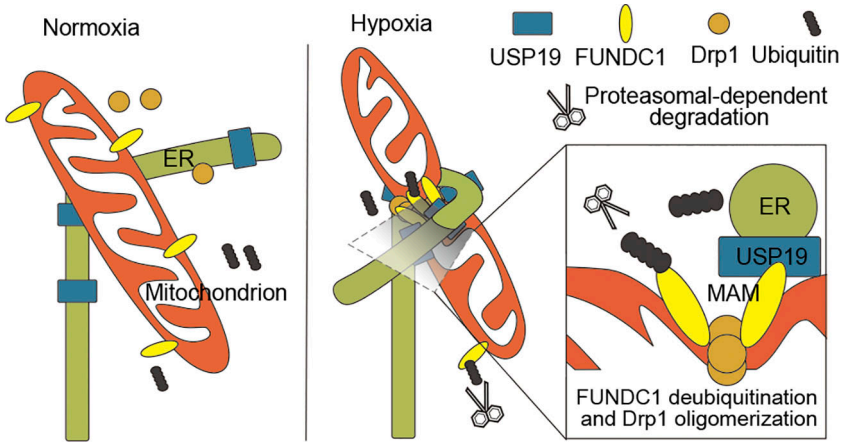

Figure 6. **Schematic of USP19 promotion of hypoxia-induced mitochondrial fission.** Under hypoxia, USP19 accumulates at ER-mitochondria contact sites with FUNDC1. USP19 interacts with and removes ubiquitin chains from FUNDC1 at ER-mitochondria contact sites. Thus, USP19 stabilizes FUNDC1 and subsequently promotes Drp1 oligomerization, leading to hypoxia-induced mitochondrial division.

Hypoxia has been shown to facilitate actin filament formation by inactivating cofilin (Vogel et al., 2010; Zieseniss, 2014). Since USP19 stabilizes HIF1α under hypoxia (Altun et al., 2012), we do not exclude the possibility that actin filaments may also play a role in USP19-mediated mitochondrial division in response to hypoxia.

FUNDC1, as a key hypoxia-induced mitophagy receptor, is tightly regulated in a specific spatiotemporal manner by post-transcriptional modification (Liu et al., 2012). At the early stage of hypoxia, FUNDC1-mediated mitophagy activity is inhibited by its phosphorylation by Src kinase and ubiquitination-mediated degradation by MARCH5, thus protecting mitochondria from unnecessary removal (Chen et al., 2017; Liu et al., 2012). As hypoxia progresses, the interaction of FUNDC1 with Src gradually decreases and mitophagy begins (Chen et al., 2017), with FUNDC1 accumulating at ER-mitochondria contact sites (Fig. 2 B and Fig. S3 B; Wu et al., 2016). In response to hypoxia, an abundance of FUNDC1 at the ER-mitochondria contact sites stabilized by USP19 is vital for hypoxia-induced mitochondrial fragmentation (Fig. 6). Moreover, USP19 deubiquitinates FUNDC1 at K119 under hypoxia (Fig, 4 E), the same site that ubiquitinated by MARCH5 (Chen et al., 2017). As both USP19 (Fig. 2 A) and MARCH5 (Sugiura et al., 2013) are localized in the MAM, USP19 and MARCH5 may oppositely regulate the deubiquitination/ubiquitination dynamic of FUNDC1 at K119 by competitively binding to FUNDC1 under hypoxia. As hypoxia progresses further, USP19 may display a binding preference for FUNDC1, preventing FUNDC1 from binding to MARCH5 at ER-mitochondria contact sites, and, as a result, facilitate the deconjugation of the ubiquitin chains from FUNDC1, stabilizing FUNDC1 to ensure hypoxia-induced mitochondrial division. This model should be validated in future studies.

Apart from USP19, depletion of USP30, a mitochondrial outer membrane deubiquitinase, also results in mitochondrial elongation (Nakamura and Hirose, 2008). An interesting question is why USP19, an ER-associated deubiquitinase, is also employed to regulate mitochondrial morphology. Distinct from USP30 inhibition of mitochondrial fusion (Yue et al., 2014), USP19 is now known to promote mitochondrial division. In addition, USP30 is highly expressed in the brain and reproductive organs (Nakamura and Hirose, 2008), while USP19 is specifically expressed in skeletal and heart muscle (Combaret et al., 2005); therefore, it is reasonable to hypothesize that USP30 and USP19 function in a tissue-specific manner. These two deubiquitinases may also respond to diverse physiological and pathological cellular environments. For example, USP30 responds to Parkinson's disease–associated acute mitochondrial depolarization (Bingol et al., 2014), while USP19 appears to respond to hypoxia. The distinct physiological functions and regulatory mechanisms of USP30 and USP19 remain to be clarified.

One mitochondrion dividing into smaller mitochondria to suit the size of an autophagosome is the premise of mitophagy (Mao and Klionsky, 2013; Tatsuta and Langer, 2008). USP19 has been reported to be a positive regulator of autophagy through stabilization of Beclin-1, the key initiation protein in autophagy (Jin et al., 2016), while Beclin-1 accumulates at the ER-mitochondria contact sites under starvation (Hamasaki et al., 2013). Given our finding that USP19 functions as a positive regulator of hypoxia-induced mitochondrial fragmentation, it will be interesting to investigate whether USP19 binds to and deubiquitinates Beclin-1 at the ER-mitochondria contact sites to promote hypoxia-induced mitophagy, thereby functioning as a vital linker that integrates mitochondrial fission and autophagy in response to hypoxia.

Materials and methods

Cell culture

HeLa and HEK293T cells were cultured in DMEM (41966; Gibco) supplemented with 10% FBS (SA201.01; CellMax) at 37°C in 5% CO_2. For hypoxia treatment, cells were transferred to a hypoxic chamber (Billups-Rothenberg) or anaerobic chamber system (Thermo Forma) at 37°C with a preanalyzed gas mixture containing 1% O_2, 5% CO_2, and 94% N_2.

Plasmids and cell transfections

The HA-USP19 plasmid was kindly provided by Dr. Yide Mei (University of Science and Technology of China, Hefei, China). Mid49 and Mid51 plasmids were kindly provided by Dr. Fei Sun (Institute of Biophysics of the Chinese Academy of Science, Beijing, China). The pSIN-C-Flag-IRES-PURO plasmid was kindly provided by Dr. Zhengfan Jiang (College of Life Science,

Peking University, Beijing, China). Sequences encoding human FUNDC1, Drp1, Fis1, and Mff transcripts were amplified from HEK293T cell cDNA and cloned into the p3×Flag-CMV-7.1 (Sigma-Aldrich), pcDNA3.1 (+) (Invitrogen), pET-28a (Novagen), or pGEX-6p-1 (GE Healthcare) vector. USP19, FUNDC1, and Drp1 mutants were constructed by overlap extension PCR. FUNDC1-Flag and FUNDC1 K119R-Flag were cloned into the pSIN-C-Flag-IRES-PURO vector.

Polyethylenimine was used to transiently transfect cells when they reached 50% to 70% confluence. After transfection for 6 h, medium was replaced with fresh medium.

Antibodies

The following antibodies were used in the present study: Rabbit anti-USP19 (25768–1-AP; ProteinTech), rabbit anti-CNX (10427–2-AP; ProteinTech), rabbit anti-FACL4 (22401–1-AP; ProteinTech), rabbit anti-VDAC1 (ab14734; Abcam), rabbit anti-VDAC2 (GTX114876; Genetex), mouse anti-MFN2 (sc-100560; Santa Cruz Biotechnology), rabbit anti-USP30 (GTX87959; Genetex), rabbit anti-FUNDC1 (GTX45570; Genetex), rabbit anti-TOM20 (11802–1-AP; ProteinTech), mouse anti-TOM20 (612278; BD Biosciences), rabbit anti-Drp1 (12957–1-AP; ProteinTech), mouse anti-DLP1 (611113; BD Biosciences), rabbit anti-HIF1α (20960–1-AP; ProteinTech), rabbit anti-PEX14 (10594–1-AP; ProteinTech), mouse anti-HA (H9658; Sigma-Aldrich), mouse anti-Flag (F1804; Sigma-Aldrich), rabbit anti-Flag (20543–1-AP; ProteinTech), mouse anti-V5 (R960CUS; Innovative Research), rabbit anti-ubiquitin (10201–2-AP; ProteinTech), mouse anti-GAPDH (60004–1-lg; ProteinTech), mouse anti–γ-tubulin (T5192; Sigma-Aldrich), peroxidase-AffiniPure goat anti-rabbit IgG (H+L) (111–035-003; Jackson ImmunoResearch), peroxidase-AffiniPure goat anti-mouse IgG (H+L) (115–035-003; Jackson ImmunoResearch), goat anti-mouse IgG (H+L) highly cross-adsorbed secondary antibody, Alexa Fluor 488 (A-11029; Invitrogen), goat anti-rabbit IgG (H+L) highly cross-adsorbed secondary antibody, Alexa Fluor 488 (A-11034; Invitrogen), and goat anti-rabbit IgG (H+L) highly cross-adsorbed secondary antibody, Alexa Fluor 568 (A-11031; Invitrogen). The anti-FUNDC1 antibody used for immune-EM was kindly provided by Dr. Quan Chen (Institute of Zoology of the Chinese Academy of Science, Beijing, China).

Generation of KO and knock-in cell lines

All of the KO cell lines were generated using a CRISPR/Cas9 approach (Ran et al., 2013). The target oligonucleotides (5′-CCA GGACTGGAGGACACCAC-3′ and 5′-GCAGAAGGATCGAGCAAA CC-3′ for USP19, 5′-CTTAAGCACTTTGTCACTGC-3′ for MFN2, 5′-GTAGCTACCCAGATTGTAAT-3′ for FUNDC1, and 5′-GCTAGA AAGCCTGGTGGGGA-3′ for Drp1) were synthesized and ligated into the gRNA vectors. HeLa cells were then transfected with gRNA plasmids, together with the Cas9 and pEGFP-C2 plasmids. Four days later, GFP-positive cells were selected and monocloned by flow cytometry (MoFlo XDP; Beckman Coulter). The expanded clones were screened by Western blotting and genome sequencing.

To generate 3×Flag-mNeonGreen-USP19 knock-in HeLa cell lines, HeLa cells were transfected with two independent target oligos (5′-ACCAAGCGGCTCAAGATGTC-3′ and 5′-AAGCGGCTC AAGATGTCTGG-3′), ligated into the gRNA vector, and an arm sequence (3×Flag-mNeonGreen flanked by 1 kb homologous sequence of the *USP19* genome) was constructed into the pcDNA3.1 vector. Seven days after transfection, cells were monocloned by flow cytometry (MoFlo XDP; Beckman Coulter) and seeded onto 96-well plates. Successful knock-in cells were confirmed by Western blotting.

Western blotting

Samples were resolved by SDS-PAGE and transfected to polyvinylidene difluoride membranes (Millipore), which were then incubated with primary antibodies and HRP-conjugated secondary antibodies. The membranes were exposed and developed using a film processing machine (Kodak).

Fluorescence microcopy

Cells were grown to 70% confluence on a coverslip, fixed in 4% paraformaldehyde for 15 min at 37°C, and then permeabilized with 0.15% Triton X-100 for 10 min. Cells were blocked with 3% BSA (900.022; Aurion) for 30 min, incubated with primary antibodies at RT for 2 h, and further incubated with secondary antibodies at RT for 1 h. Samples were observed under a confocal microscope (Leica TCS SP8) equipped with a 100 × 1.4 NA oil objective lens. Images were acquired using LAS X software (Leica).

EM

HeLa cells at 80% confluency were fixed using 2% paraformaldehyde and 2% glutaraldehyde in PBS buffer (pH 7.4) at RT for 1 h. Samples were washed three times each for 10 min with sodium cacodylate buffer and were postfixed in 1.2% osmium tetroxide and 1.5% potassium ferrocyanide on ice for 30 min. Cells were then stained with 1% uranyl acetate in 50% ethanol at RT for 1 h. All samples were dehydrated through graded alcohol (65%, 75%, 85%, 95%, and 100%) and embedded in epon 812 (SPI-Chem). Serial sections were cut on a Leica UC7 Ultramicrotome and stained with uranyl acetate and lead citrate for 20 min and 10 min, respectively. Images were collected with an electron microscope (FEI Tecnai G2 Spirit) at 120 kV.

For preembedding immune-EM, experiments were performed as described previously (Polishchuk and Mironov, 2001). Briefly, cells were fixed by adding fixative (4% paraformaldehyde in 0.2 M Hepes buffer [pH 7.4]) to the cell culture medium (1:1) for 5 min at RT. The combined fixative was removed and replaced with postfixative for 30 min. Cells were washed in PBS three times for 5 min each and preincubated in blocking/permeabilizing solution containing 0.5% BSA, 0.1% saponin, and 50 mM NH_4Cl in PBS for 30 min. Cells were subsequently incubated with primary anti-Flag (20543–1-AP; 1:1,000; ProteinTech) or anti-FUNDC1 (1:25) antibody in blocking/permeabilizing solution on a shaker for 1 h at RT and held overnight at 4°C. Cells were rinsed five times for 5 min each with PBS at RT and kept overnight at 4°C. Following several washes in PBS, immunogold-labeled cells were fixed with 1% glutaraldehyde in 0.2 M Hepes buffer (pH 7.4) for 30 min, 50 mM glycine-PBS was used for quenching the free aldehyde, followed by three 5-min

washes in PBS and three 5-min washes in Milli-Q water. Gold particles were intensified using a GoldEnhance EM Plus kit (2114; Nanoprobes) for 2 min at RT. Labeled cells were washed with Milli-Q water three times, osmicated (1% OsO_4 and 1.5% $K_4Fe(CN)_6$) in 0.1 M cacodylate buffer on ice for 1 h, stained with 2% uranyl acetate in Milli-Q water, dehydrated twice with an ethanol series (30%, 50%, 70%, 85%, 95%, and 100%) for 5 min each, and then embedded in Embed 812 resin (14120; EMS). Plastic sections (70-nm thick) were obtained using a Leica UC7 Ultramicrotome and collected on formvar film-coated copper grids with a single slot. Sections were poststained with 2% saturated uranyl acetate in 50% ethanol and 1% lead citrate. The resin sections were examined at 120 kV on a Tecnai G^2 Spirit BioTWIN (FEI) transmission electron microscope equipped with a Gatan 832 CCD camera (Gatan).

Live cell imaging and mito-PAGFP assay

For live cell imaging, HeLa cells were exposed to hypoxia for 6 h and incubated for 30 min with 50 nM MitoTracker Red (M7512; Thermo Fisher Scientific), washed twice with PBS buffer, and replenished with fresh media. The imaging experiment was performed using a spinning-disk UltraVIEW VoX imaging system (PerkinElmer) equipped with a 60 × 1.4 NA objective lens. For time tracking, cells were observed in a chamber at 37°C under 1% O_2 and images were postprocessed using the Velocity (Nikon) software.

For mitochondrial fusion assays, HeLa cells transfected with mito-PAGFP were imaged using a spinning-disk UltraVIEW VoX microscope system with a 60 × 1.4 NA objective lens. Four-µm-wide ROIs were selected and activated by a single-pulse 405-nm laser. The green fluorescent z-stacks were acquired before and immediately following activation and then every 5 min for 30 min

GST- or His-tag fusion protein production

GST- or His-tagged fusion proteins were expressed in the *Escherichia coli* BL21 strain (200131; Stratagene/Agilent). For GST-FUNDC1 protein expression, logarithmic phase BL21 cells were induced by the addition of 1 mM IPTG (J436; Amresco) and incubated overnight at 18°C. Cells were harvested and lysed ultrasonically in GST pull-down buffer (20 mM Tris-HCl [pH 7.6], 150 mM NaCl, and 0.5% Triton X-100) and GST-FUNDC1 was purified using Glutathione Sepharose 4B beads (17075601; GE Healthcare). For 6×His-USP19ΔTMD protein expression, BL21 cells were induced with 0.5 mM IPTG and incubated overnight at 24°C. Cells were harvested and lysed ultrasonically in buffer (50 mM Tris-HCl [pH 8.0], 300 mM NaCl, 4 mM imidazole, and 2 mM β-mercaptoethanol) and His fusion proteins were purified using Ni-NTA beads (30210; GE Healthcare). Fusion protein-bound beads were used in pull-down assays.

Immunoprecipitation and GST pull-down assay

For immunoprecipitation, cells were washed three times in cold PBS buffer and lysed on ice for 30 min in immunoprecipitation buffer (25 mM Hepes [pH 7.4], 150 mM KAc, 2 mM $Mg(Ac)_2$, and 0.5% Triton X-100) containing protease inhibitor cocktail. After centrifugation at 12,000 × *g* for 15 min at 4°C, lysates were incubated with the relevant antibody for 2 h at 4°C and then incubated with Protein G-Sepharose beads (17061801; GE Healthcare) for 2 h. After washing five times in immunoprecipitation buffer, the beads were boiled in SDS loading buffer and the samples were analyzed by Western blotting.

For pull-down assays, HEK293T cells transfected with HA-USP19 were lysed in cell lysis buffer (50 mM Tris-HCl [pH 7.4], 150 mM NaCl, 1% NP-40, and 10% glycerol) containing protease inhibitor cocktail. After centrifugation at 12,000 × *g* for 10 min at 4°C, the lysates were incubated with GST- or GST-FUNDC1-bound beads for 2 h at 4°C. The beads were washed three times and boiled at 100°C for 5 min in SDS loading buffer, and the samples were analyzed by Western blotting using an anti-HA antibody or by Coomassie blue staining.

In vitro deubiquitination assay

HEK293T cells cotransfected with HA-Ub and Flag-FUNDC1 were harvested and lysed in lysis buffer (50 mM Tris-HCl [pH 7.8], 150 mM NaCl, 10 mM NaF, 1 mM EDTA, 1% Triton X-100, 0.2% sarcosyl, 1 mM DTT, and 10% glycerol) containing protease inhibitor cocktail. After centrifugation at 12,000 × *g* for 10 min at 4°C, the supernatant was incubated with Protein G-Sepharose beads conjugated with an anti-Flag antibody for 2 h at 4°C. Ubiquitinated FUNDC1 was eluted using Flag peptides. The recombinant 3×Flag-USP19 and its mutant were expressed in HEK293T cells and purified using beads conjugated with an anti-Flag antibody and eluted using 3×Flag peptides. Ubiquitinated FUNDC1 protein was incubated with USP19 or its mutant in deubiquitination buffer (50 mM Tris-HCl [pH 8.0], 50 mM NaCl, 1 mM EDTA, 10 mM DTT, and 5% glycerol) for 2 h at 37°C. Samples were analyzed by Western blotting.

Subcellular fractionation

The procedure used for subcellular fractionation was conducted as described in two previous reports (Frezza et al., 2007; Wieckowski et al., 2009). Briefly, mouse skeletal muscle was resuspended in ice-cold PBS supplemented with 10 mM EDTA and 0.1% trypsin for 30 min at 4°C and then centrifuged at 200 × *g* for 5 min at 4°C. Cells were resuspended in ice-cold IB_{cell}-1 buffer (30 mM Tris-HCl [pH 7.4], 225 mM mannitol, 75 mM sucrose, and 0.1 mM EGTA) and gently disrupted using a Dounce homogenizer. The homogenate was centrifuged twice at 600 × *g* for 5 min at 4°C, and the supernatant was subsequently centrifuged at 7,000 × *g* for 10 min at 4°C to pellet the crude mitochondrial fraction. The resultant supernatant was further centrifuged at 100,000 × *g* for 1 h at 4°C (Beckman 70-Ti rotor) to separate the ER (pellet) and cytosolic fraction (supernatant). The crude mitochondrial pellet was gently resuspended in 2 ml of ice-cold MRB buffer (250 mM mannitol [pH 7.4], 5 mM Hepes, and 0.5 mM EGTA), layered on 8 ml of Percoll medium (225 mM mannitol [pH 7.4], 25 mM Hepes, 1 mM EGTA, and 30% Percoll [vol/vol]) in a 14-ml thin-wall Polyallomer ultracentrifuge tube, and centrifuged at 95,000 × *g* for 30 min at 4°C (Beckman SW40 rotor) to separate the MAM and pure mitochondria. The quality of the subcellular fractionation was evaluated by Western blotting.

PLA

Cells were subjected to the PLA assay (Sigma-Aldrich) according to the manufacturer's instructions using anti-Flag and anti-VDAC1 or anti-CNX and anti-TOM20 antibodies. Samples were observed under a confocal microscope (Leica TCS SP8) equipped with a 100 × 1.4 NA oil objective lens. The number of PLA-positive dots was quantified using the particle analysis function in ImageJ software (National Institutes of Health) and expressed as dots per cell.

Drp1 oligomerization assay

Crude mitochondrial fractions from hypoxic HeLa cells were lysed in digitonin buffer (50 mM Tris-HCl [pH 7.4], 150 mM NaCl, 1 mM $MgOAc_2$, 1 mM DTT, 1 mM GTP, and 1% digitonin) containing protease inhibitor cocktail and centrifuged at 12,000 × *g* for 10 min at 4°C. Lysates were layered on 1.2 ml of 15% to 35% (wt/vol) sucrose gradient buffer (50 mM Tris-HCl [pH 7.4] and 150 mM NaCl) containing protease inhibitor cocktail and centrifuged at 170,0000 × *g* for 12 h at 4°C. The centrifuged gradient was separated into 13 fractions and analyzed by Western blotting.

GTP-binding assay

Crude mitochondrial fractions from hypoxic HeLa cells or Drp1 KO cells overexpressing Drp1 plasmids were lysed in digitonin buffer (50 mM Tris-HCl [pH 7.4], 150 mM NaCl, and 1% digitonin) containing protease inhibitor cocktail. After centrifugation at 12,000 × *g* for 10 min at 4°C, lysates were incubated on ice or at 30°C for 60 min with GTP-agarose beads (G9768; Sigma-Aldrich) in reaction buffer (50 mM Tris-HCl [pH 7.4], 150 mM NaCl, 1 mM $MgOAc_2$, and 1 mM DTT) containing protease inhibitor cocktail. After washing three times in reaction buffer, proteins were eluted using elution buffer (1% digitonin, 50 mM Tris-HCl [pH 7.4], 150 mM NaCl, and 10 mM GTP) containing protease inhibitor cocktail for 1 h at 4°C. 4× SDS-PAGE sample buffer was added to the eluates containing GTP-agarose (G9768; Sigma-Aldrich). Samples were analyzed by Western blotting.

GTP hydrolysis assay

Drp1 was purified from crude mitochondrial fractions or Drp1 KO cells overexpressing Drp1 plasmids by immunoprecipitation using an anti-Drp1 antibody. The purified proteins were incubated with 30 µl 20 mM Hepes-KOH buffer (pH 7.4) containing 2 mM $MgCl_2$, 1 mM DTT, and 1% Triton X-100 with 1 µCi [α-32P] GTP (cat. no. NEG506H; PerkinElmer) at 37°C for 10 min. One microliter of the reaction mixture was spotted on a polythyleneimine-cellulose filter (105579; Merck) and resolved by TLC in 1 M LiCl and 2 M formic acid. The products were analyzed and quantified using a Bioimage Analyzer BAS2000 (BAS2000; FujiFilm).

Quantification and statistical analysis

Statistical data were analyzed using unpaired two-tailed Student's *t* tests and represented as mean ± SEM. Asterisks represent corresponding statistical significance: *, $P < 0.05$; **, $P < 0.01$; and ***, $P < 0.001$. Statistical details for each experiment, including statistical significance and *n* value, are provided in the figure legends. The Shapiro-Wilk test was employed to evaluate the normal distribution of the data. Statistical analyses and data plotting were performed using GraphPad Prism 6. Sample preparation was not blind, but quantification was performed in a blinded manner. No sample size estimations were performed, no strategy for randomization and/or stratification was employed, and no data or subjects were excluded from the analysis. All experiments were performed three times.

Online supplemental material

Fig. S1 shows the establishment of USP19 KO HeLa cells. Fig. S2 illustrates that USP19 does not affect ER morphology, peroxisome number, or mitochondrial fusion rate under hypoxia. Fig. S3 depicts USP19 accumulating in the MAM under hypoxia along with FACL4, Drp1, and FUNDC1, but not affecting the tethering of the ER to mitochondria. Fig. S4 shows that USP19 neither interacts with Mff, Fis1, MiD49, or MiD51, nor affects their stabilities. Fig. S5 illustrates that USP19 interacts with Drp1, and the Drp1 R403C mutant impairs GTPase activity.

Acknowledgments

We thank Dr. Jingwei Xiong at the Institute of Molecular Medicine of Peking University (Beijing, China) for providing the Cas9 and gRNA plasmids; we also thank Drs. Chunyan Shan, Pengyuan Dong, Yunchao Xie, Wei Pan, and Shitang Huang at the Core Facilities of Life Sciences of Peking University (Beijing, China) for their assistance with confocal imaging, EM sample preparation and image analysis, ultracentrifugation, GTP hydrolysis assays, and statistical analysis. We thank the flow cytometry Core at National Center for Protein Sciences at Peking University, particularly Drs. Liying Du and Hongxia Lu, for technical help.

This work was supported by the National Natural Science Foundation of China (grants 91954124 and 31871353) and the National Key Research and Development Program of China Stem Cell and Translational Research (grant 2016YFA0100501).

The authors declare no competing financial interests.

Author contributions: P. Chai conceived and designed the project; P. Chai, Y. Cheng, C. Hou, L. Yin, D. Zhang, and Y. Hu conducted the experiments; P. Chai, Y. Cheng, Q. Chen, and P. Zheng performed the statistical analysis; J. Teng and J. Chen supervised the work; all authors interpreted and analyzed the data; P. Chai, J. Teng, and J. Chen wrote the manuscript.

Submitted: 2 October 2020
Revised: 10 March 2021
Accepted: 19 April 2021

References

Altun, M., B. Zhao, K. Velasco, H. Liu, G. Hassink, J. Paschke, T. Pereira, and K. Lindsten. 2012. Ubiquitin-specific protease 19 (USP19) regulates hypoxia-inducible factor 1α (HIF-1α) during hypoxia. *J. Biol. Chem.* 287: 1962–1969. https://doi.org/10.1074/jbc.M111.305615

Bingol, B., J.S. Tea, L. Phu, M. Reichelt, C.E. Bakalarski, Q. Song, O. Foreman, D.S. Kirkpatrick, and M. Sheng. 2014. The mitochondrial deubiquitinase USP30 opposes parkin-mediated mitophagy. *Nature.* 510:370–375. https://doi.org/10.1038/nature13418

Chan, D.C. 2012. Fusion and fission: interlinked processes critical for mitochondrial health. *Annu. Rev. Genet.* 46:265–287. https://doi.org/10.1146/annurev-genet-110410-132529

Chen, H., and D.C. Chan. 2017. Mitochondrial Dynamics in Regulating the Unique Phenotypes of Cancer and Stem Cells. *Cell Metab.* 26:39–48. https://doi.org/10.1016/j.cmet.2017.05.016

Chen, Z., L. Liu, Q. Cheng, Y. Li, H. Wu, W. Zhang, Y. Wang, S.A. Sehgal, S. Siraj, X. Wang, et al. 2017. Mitochondrial E3 ligase MARCH5 regulates FUNDC1 to fine-tune hypoxic mitophagy. *EMBO Rep.* 18:495–509. https://doi.org/10.15252/embr.201643309

Combaret, L., O.A. Adegoke, N. Bedard, V. Baracos, D. Attaix, and S.S. Wing. 2005. USP19 is a ubiquitin-specific protease regulated in rat skeletal muscle during catabolic states. *Am. J. Physiol. Endocrinol. Metab.* 288: E693–E700. https://doi.org/10.1152/ajpendo.00281.2004

de Brito, O.M., and L. Scorrano. 2008. Mitofusin 2 tethers endoplasmic reticulum to mitochondria. *Nature.* 456:605–610. https://doi.org/10.1038/nature07534

Fahrner, J.A., R. Liu, M.S. Perry, J. Klein, and D.C. Chan. 2016. A novel de novo dominant negative mutation in DNM1L impairs mitochondrial fission and presents as childhood epileptic encephalopathy. *Am. J. Med. Genet. A.* 170:2002–2011. https://doi.org/10.1002/ajmg.a.37721

Frezza, C., S. Cipolat, and L. Scorrano. 2007. Organelle isolation: functional mitochondria from mouse liver, muscle and cultured fibroblasts. *Nat. Protoc.* 2:287–295. https://doi.org/10.1038/nprot.2006.478

Friedman, J.R., L.L. Lackner, M. West, J.R. DiBenedetto, J. Nunnari, and G.K. Voeltz. 2011. ER tubules mark sites of mitochondrial division. *Science.* 334:358–362. https://doi.org/10.1126/science.1207385

Gandre-Babbe, S., and A.M. van der Bliek. 2008. The novel tail-anchored membrane protein Mff controls mitochondrial and peroxisomal fission in mammalian cells. *Mol. Biol. Cell.* 19:2402–2412. https://doi.org/10.1091/mbc.e07-12-1287

Hamasaki, M., N. Furuta, A. Matsuda, A. Nezu, A. Yamamoto, N. Fujita, H. Oomori, T. Noda, T. Haraguchi, Y. Hiraoka, et al. 2013. Autophagosomes form at ER-mitochondria contact sites. *Nature.* 495:389–393. https://doi.org/10.1038/nature11910

Hassink, G.C., B. Zhao, R. Sompallae, M. Altun, S. Gastaldello, N.V. Zinin, M.G. Masucci, and K. Lindsten. 2009. The ER-resident ubiquitin-specific protease 19 participates in the UPR and rescues ERAD substrates. *EMBO Rep.* 10:755–761. https://doi.org/10.1038/embor.2009.69

Hatch, A.L., W.K. Ji, R.A. Merrill, S. Strack, and H.N. Higgs. 2016. Actin filaments as dynamic reservoirs for Drp1 recruitment. *Mol. Biol. Cell.* 27: 3109–3121. https://doi.org/10.1091/mbc.e16-03-0193

Ingerman, E., E.M. Perkins, M. Marino, J.A. Mears, J.M. McCaffery, J.E. Hinshaw, and J. Nunnari. 2005. Dnm1 forms spirals that are structurally tailored to fit mitochondria. *J. Cell Biol.* 170:1021–1027. https://doi.org/10.1083/jcb.200506078

Ji, W.K., A.L. Hatch, R.A. Merrill, S. Strack, and H.N. Higgs. 2015. Actin filaments target the oligomeric maturation of the dynamin GTPase Drp1 to mitochondrial fission sites. *eLife.* 4:e11553. https://doi.org/10.7554/eLife.11553

Ji, W.K., R. Chakrabarti, X. Fan, L. Schoenfeld, S. Strack, and H.N. Higgs. 2017. Receptor-mediated Drp1 oligomerization on endoplasmic reticulum. *J. Cell Biol.* 216:4123–4139. https://doi.org/10.1083/jcb.201610057

Jin, S., S. Tian, Y. Chen, C. Zhang, W. Xie, X. Xia, J. Cui, and R.F. Wang. 2016. USP19 modulates autophagy and antiviral immune responses by deubiquitinating Beclin-1. *EMBO J.* 35:866–880. https://doi.org/10.15252/embj.201593596

Karbowski, M., D. Arnoult, H. Chen, D.C. Chan, C.L. Smith, and R.J. Youle. 2004. Quantitation of mitochondrial dynamics by photolabeling of individual organelles shows that mitochondrial fusion is blocked during the Bax activation phase of apoptosis. *J. Cell Biol.* 164:493–499. https://doi.org/10.1083/jcb.200309082

Kenneth, N.S., and S. Rocha. 2008. Regulation of gene expression by hypoxia. *Biochem. J.* 414:19–29. https://doi.org/10.1042/BJ20081055

Kim, H., M.C. Scimia, D. Wilkinson, R.D. Trelles, M.R. Wood, D. Bowtell, A. Dillin, M. Mercola, and Z.A. Ronai. 2011. Fine-tuning of Drp1/Fis1 availability by AKAP121/Siah2 regulates mitochondrial adaptation to hypoxia. *Mol. Cell.* 44:532–544. https://doi.org/10.1016/j.molcel.2011.08.045

Komander, D., and M. Rape. 2012. The ubiquitin code. *Annu. Rev. Biochem.* 81: 203–229. https://doi.org/10.1146/annurev-biochem-060310-170328

Korobova, F., V. Ramabhadran, and H.N. Higgs. 2013. An actin-dependent step in mitochondrial fission mediated by the ER-associated formin INF2. *Science.* 339:464–467. https://doi.org/10.1126/science.1228360

Lee, J.G., S. Takahama, G. Zhang, S.I. Tomarev, and Y. Ye. 2016. Unconventional secretion of misfolded proteins promotes adaptation to proteasome dysfunction in mammalian cells. *Nat. Cell Biol.* 18:765–776. https://doi.org/10.1038/ncb3372

Liu, L., D. Feng, G. Chen, M. Chen, Q. Zheng, P. Song, Q. Ma, C. Zhu, R. Wang, W. Qi, et al. 2012. Mitochondrial outer-membrane protein FUNDC1 mediates hypoxia-induced mitophagy in mammalian cells. *Nat. Cell Biol.* 14:177–185. https://doi.org/10.1038/ncb2422

Losón, O.C., Z. Song, H. Chen, and D.C. Chan. 2013. Fis1, Mff, MiD49, and MiD51 mediate Drp1 recruitment in mitochondrial fission. *Mol. Biol. Cell.* 24:659–667. https://doi.org/10.1091/mbc.e12-10-0721

Mao, K., and D.J. Klionsky. 2013. Mitochondrial fission facilitates mitophagy in Saccharomyces cerevisiae. *Autophagy.* 9:1900–1901. https://doi.org/10.4161/auto.25804

Mei, Y., A.A. Hahn, S. Hu, and X. Yang. 2011. The USP19 deubiquitinase regulates the stability of c-IAP1 and c-IAP2. *J. Biol. Chem.* 286: 35380–35387. https://doi.org/10.1074/jbc.M111.282020

Mishra, P., and D.C. Chan. 2014. Mitochondrial dynamics and inheritance during cell division, development and disease. *Nat. Rev. Mol. Cell Biol.* 15: 634–646. https://doi.org/10.1038/nrm3877

Nakamura, N., and S. Hirose. 2008. Regulation of mitochondrial morphology by USP30, a deubiquitinating enzyme present in the mitochondrial outer membrane. *Mol. Biol. Cell.* 19:1903–1911. https://doi.org/10.1091/mbc.e07-11-1103

Otera, H., C. Wang, M.M. Cleland, K. Setoguchi, S. Yokota, R.J. Youle, and K. Mihara. 2010. Mff is an essential factor for mitochondrial recruitment of Drp1 during mitochondrial fission in mammalian cells. *J. Cell Biol.* 191: 1141–1158. https://doi.org/10.1083/jcb.201007152

Polishchuk, R.S., and A.A. Mironov. 2001. Correlative video light/electron microscopy. Curr. Protoc. Cell Biol. 11:4.8.1–4.8.9.

Ran, F.A., P.D. Hsu, J. Wright, V. Agarwala, D.A. Scott, and F. Zhang. 2013. Genome engineering using the CRISPR-Cas9 system. *Nat. Protoc.* 8: 2281–2308. https://doi.org/10.1038/nprot.2013.143

Rehklau, K., L. Hoffmann, C.B. Gurniak, M. Ott, W. Witke, L. Scorrano, C. Culmsee, and M.B. Rust. 2017. Cofilin1-dependent actin dynamics control DRP1-mediated mitochondrial fission. *Cell Death Dis.* 8:e3063. https://doi.org/10.1038/cddis.2017.448

Romanello, V., E. Guadagnin, L. Gomes, I. Roder, C. Sandri, Y. Petersen, G. Milan, E. Masiero, P. Del Piccolo, M. Foretz, et al. 2010. Mitochondrial fission and remodelling contributes to muscle atrophy. *EMBO J.* 29: 1774–1785. https://doi.org/10.1038/emboj.2010.60

Smirnova, E., D.L. Shurland, S.N. Ryazantsev, and A.M. van der Bliek. 1998. A human dynamin-related protein controls the distribution of mitochondria. *J. Cell Biol.* 143:351–358. https://doi.org/10.1083/jcb.143.2.351

Sugiura, A., S. Nagashima, T. Tokuyama, T. Amo, Y. Matsuki, S. Ishido, Y. Kudo, H.M. McBride, T. Fukuda, N. Matsushita, et al. 2013. MITOL regulates endoplasmic reticulum-mitochondria contacts via Mitofusin2. *Mol. Cell.* 51:20–34. https://doi.org/10.1016/j.molcel.2013.04.023

Tatsuta, T., and T. Langer. 2008. Quality control of mitochondria: protection against neurodegeneration and ageing. *EMBO J.* 27:306–314. https://doi.org/10.1038/sj.emboj.7601972

Vogel, S., M. Wottawa, K. Farhat, A. Zieseniss, M. Schnelle, S. Le-Huu, M. von Ahlen, C. Malz, G. Camenisch, and D.M. Katschinski. 2010. Prolyl hydroxylase domain (PHD) 2 affects cell migration and F-actin formation via RhoA/rho-associated kinase-dependent cofilin phosphorylation. *J. Biol. Chem.* 285:33756–33763. https://doi.org/10.1074/jbc.M110.132985

Wieckowski, M.R., C. Giorgi, M. Lebiedzinska, J. Duszynski, and P. Pinton. 2009. Isolation of mitochondria-associated membranes and mitochondria from animal tissues and cells. *Nat. Protoc.* 4:1582–1590. https://doi.org/10.1038/nprot.2009.151

Wu, W., C. Lin, K. Wu, L. Jiang, X. Wang, W. Li, H. Zhuang, X. Zhang, H. Chen, S. Li, et al. 2016. FUNDC1 regulates mitochondrial dynamics at the ER-mitochondrial contact site under hypoxic conditions. *EMBO J.* 35: 1368–1384. https://doi.org/10.15252/embj.201593102

Yoon, Y., E.W. Krueger, B.J. Oswald, and M.A. McNiven. 2003. The mitochondrial protein hFis1 regulates mitochondrial fission in mammalian cells through an interaction with the dynamin-like protein DLP1. *Mol. Cell. Biol.* 23:5409–5420. https://doi.org/10.1128/MCB.23.15.5409-5420.2003

Youle, R.J., and A.M. van der Bliek. 2012. Mitochondrial fission, fusion, and stress. *Science.* 337:1062–1065. https://doi.org/10.1126/science.1219855

Yue, W., Z. Chen, H. Liu, C. Yan, M. Chen, D. Feng, C. Yan, H. Wu, L. Du, Y. Wang, et al. 2014. A small natural molecule promotes mitochondrial fusion through inhibition of the deubiquitinase USP30. *Cell Res.* 24: 482–496. https://doi.org/10.1038/cr.2014.20

Zheng, P., Q. Chen, X. Tian, N. Qian, P. Chai, B. Liu, J. Hu, C. Blackstone, D. Zhu, J. Teng, and J. Chen. 2018. DNA damage triggers tubular endoplasmic reticulum extension to promote apoptosis by facilitating ER-mitochondria signaling. *Cell Res.* 28:833–854. https://doi.org/10.1038/s41422-018-0065-z

Zieseniss, A. 2014. Hypoxia and the modulation of the actin cytoskeleton - emerging interrelations. *Hypoxia (Auckl.).* 2:11–21. https://doi.org/10.2147/HP.S53575

Supplemental material

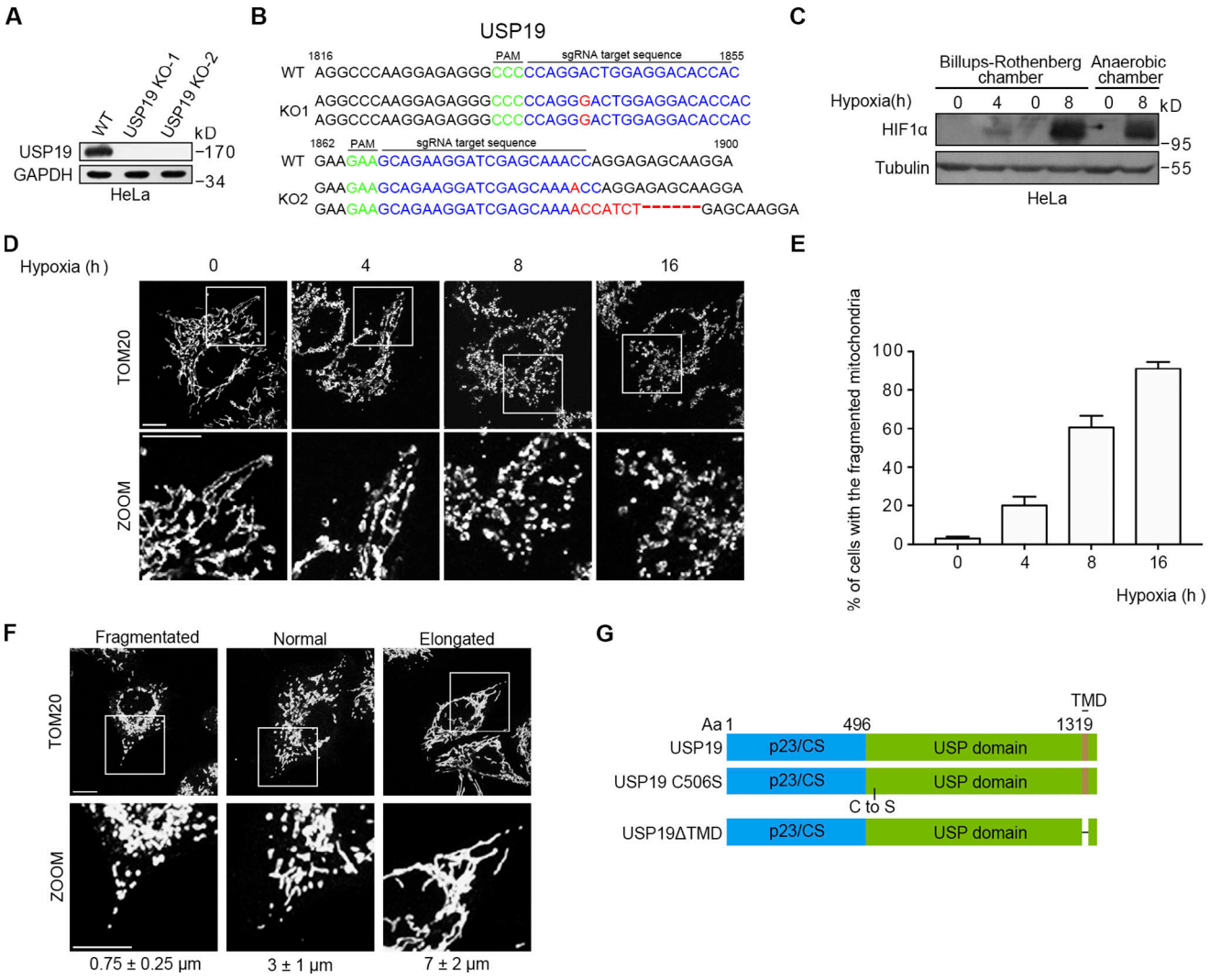

Figure S1. **Establishment of USP19 KO HeLa cell lines and hypoxia efficacy examination. (A)** Western blot analysis of lysates from WT and USP19 KO HeLa cells. GAPDH served as loading control. **(B)** Sequence alignment of partial USP19 coding sequences from WT and USP19 KO HeLa cells lines. Protospacer adjacent motif (PAM), green; sgRNA target, blue; mutated sequence, red. **(C)** Western blot analysis of lysates from HeLa cells exposed to hypoxia for the indicated time in a Billups-Rothenberg chamber or anaerobic chamber system. Tubulin served as a loading control. **(D)** Representative confocal images of mitochondrial morphology in HeLa cells exposed to hypoxia for the indicated time and immunostained for TOM20. An enlargement of the hatched box is shown on the bottom of each panel. Scale bar, 10 μm. **(E)** Quantification of the cells containing fragmented mitochondria in D. Bars represent mean ± SEM; $n \geq 100$ cells. **(F)** Representative confocal images of each category of mitochondrial morphology. Cells were immunostained for TOM20. An enlargement of the hatched box is shown. Scale bar, 10 μm. **(G)** Schematic of USP19 mutants. TMD, transmembrane domain.

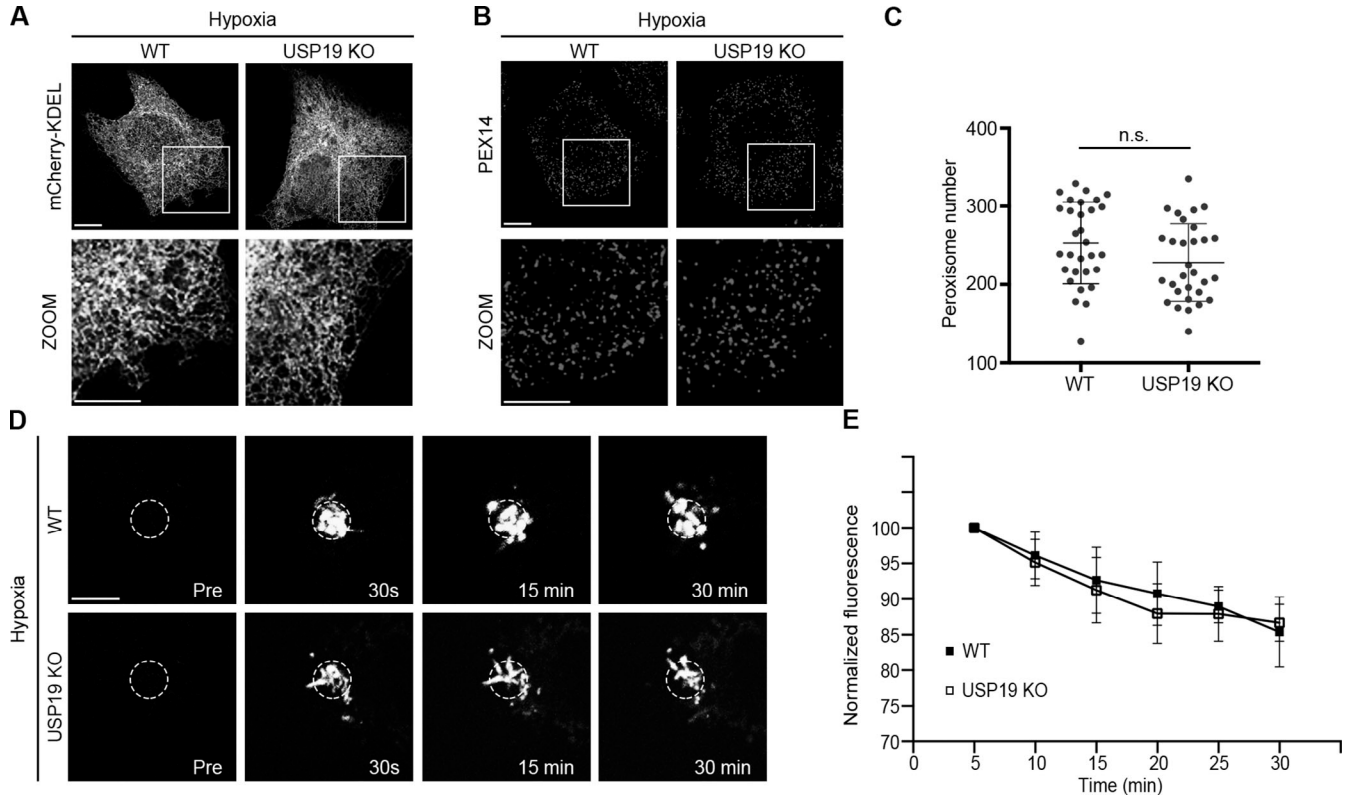

Figure S2. **USP19 deficiency does not affect ER morphology, peroxisome number, or mitochondrial fusion rate under hypoxia. (A)** Representative confocal images of the ER in WT and USP19 KO HeLa cells transfected with mCherry-KDEL and exposed to hypoxia for 8 h. An enlargement of the hatched box is shown on the bottom of each panel. Scale bar, 10 µm. **(B)** Representative confocal images of the peroxisome in WT and USP19 KO HeLa cells exposed to hypoxia for 8 h and immunostained for PEX14. An enlargement of the hatched box is shown on the bottom of each panel. Scale bar, 10 µm. **(C)** Quantification of peroxisome number in B. Bars represent mean ± SEM; unpaired two-tailed Student's *t* test, $n \geq 31$ cells. **(D)** Live cell images of WT and USP19 KO HeLa cells exposed to hypoxia for 8 h were analyzed using the mito-PAGFP mitochondrial fusion assay. Mito-PAGFP is photoactivated in the indicated ROIs, and the decrease in fluorescence is followed in the same ROI. Scale bar, 7.5 µm. **(E)** Quantification of mitochondrial fusion rates in D. Bars represent mean ± SEM; unpaired two-tailed Student's *t* test, $n \geq 12$ cells.

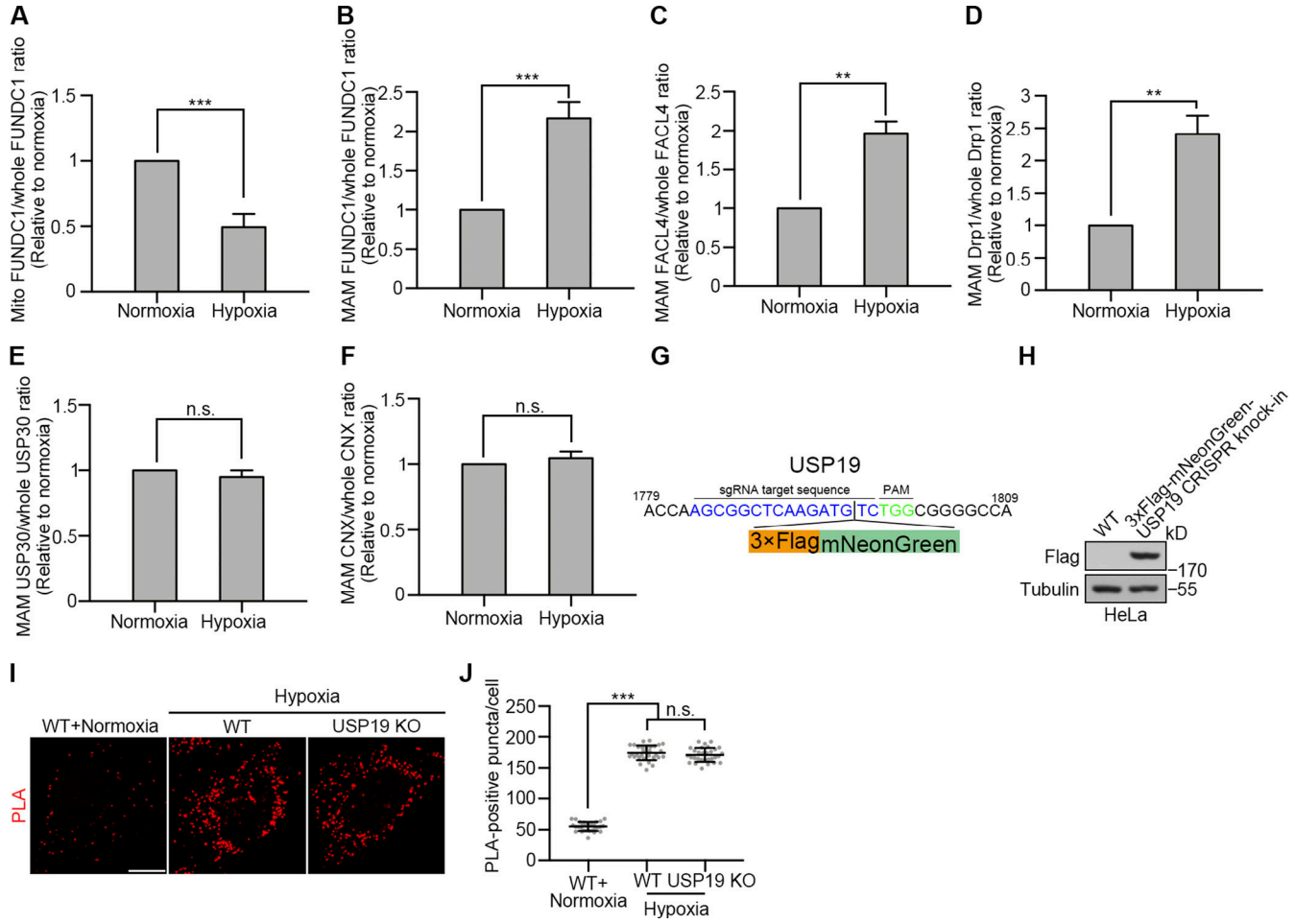

Figure S3. **USP19 accumulates in the MAM under hypoxia but does not affect the tethering of the ER to mitochondria. (A)** Quantification of the ratio of mitochondrial (mito) FUNDC1 in HeLa cells exposed to normoxia or hypoxia for 8 h. Bar represents mean ± SEM. ***, P < 0.001, unpaired two-tailed Student's *t* test, three independent experiments. **(B–F)** Quantification of the ratio of FUNDC1 (B), FACL4 (C), Drp1 (D), USP30 (E), and CNX (F) in the MAM of HeLa cells exposed to normoxia or hypoxia for 8 h. Bars represent mean ± SEM. **, P < 0.01; ***, P < 0.001, unpaired two-tailed Student's *t* test, three independent experiments. **(G)** Partial USP19 coding sequences from 3×Flag-mNeonGreen-USP19 knock-in HeLa cells. Protospacer adjacent motif (PAM), green; sgRNA target, blue. **(H)** Western blot analysis of lysates from WT and 3×Flag-mNeonGreen-USP19 knock-in HeLa cells. Tubulin served as loading control. **(I)** WT and USP19 KO HeLa cells were exposed to normoxia or hypoxia for 8 h and subjected to PLA with anti-TOM20 and anti-CNX antibodies. Projections of z-stacked representative images are shown. Scale bar, 10 µm. **(J)** Quantification of the number of PLA-positive puncta/cells in I. Bars represent mean ± SEM. ***, P < 0.001, unpaired two-tailed Student's *t* test, three independent experiments, *n* ≥ 30 cells.

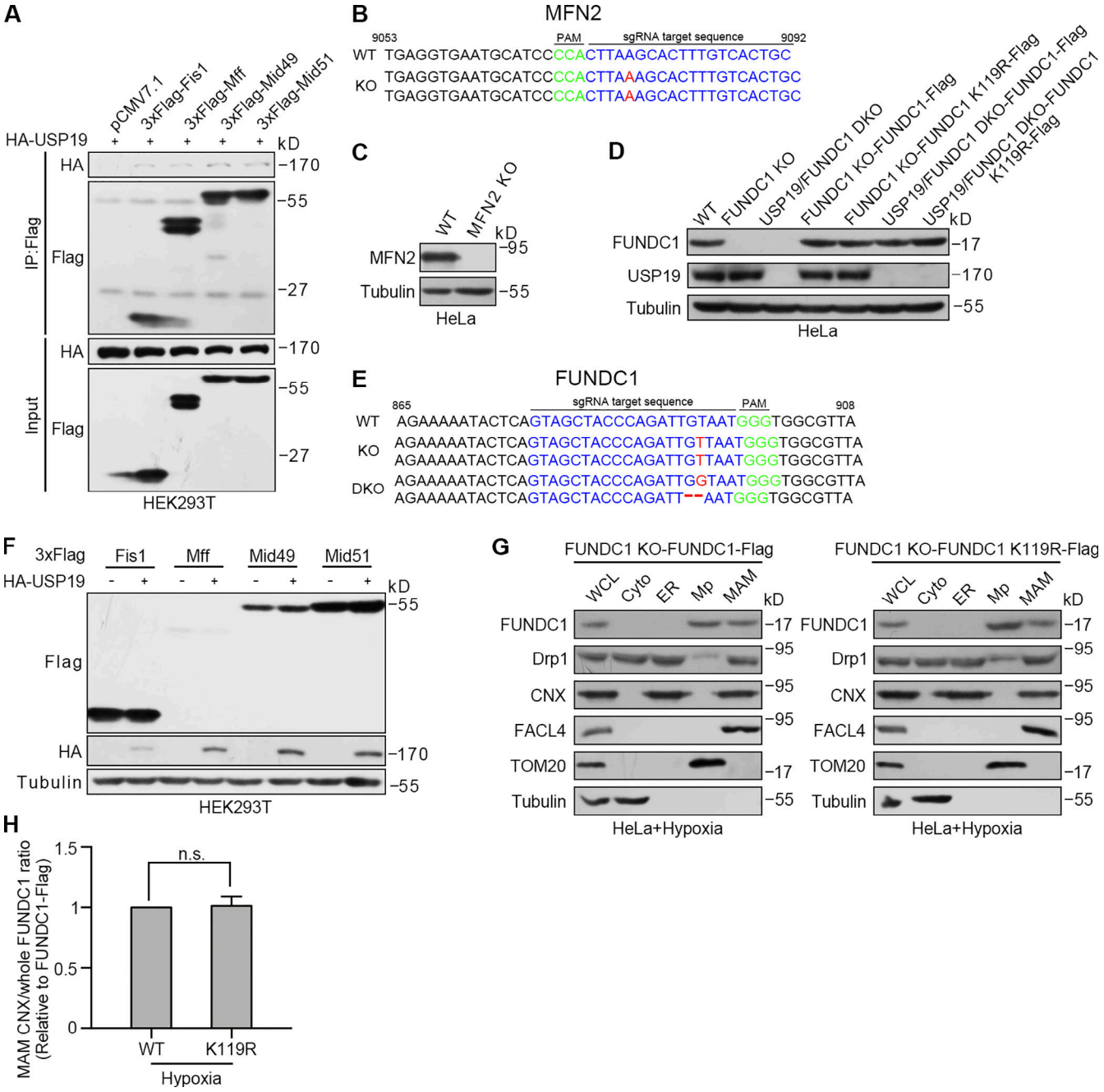

Figure S4. **USP19 neither interacts with Mff, Fis1, MiD49, or MiD51, nor affects their stabilities. (A)** Lysates from HEK293T cells cotransfected with the indicated plasmids were immunoprecipitated (IP) with an anti-Flag antibody. Immunoprecipitated samples were analyzed by Western blotting. **(B)** Sequence alignment of partial MFN2 coding sequences from WT and MFN2 KO HeLa cell lines. Protospacer adjacent motif (PAM), green; sgRNA target, blue; mutated sequence, red. **(C)** Western blot analysis of lysates from WT and MFN2 KO HeLa cells. Tubulin served as loading control. **(D)** Western blotting analysis of lysates from WT, FUNDC1 KO, USP19/FUNDC1 DKO, FUNDC1 KO, and USP19/FUNDC1 DKO HeLa cells stably expressing FUNDC1-Flag or FUNDC1 K119R-Flag (FUNDC1 KO-FUNDC1-Flag, FUNDC1 KO-FUNDC1 K119R-Flag, USP19/FUNDC1 DKO-FUNDC1-Flag, USP19/FUNDC1 DKO-FUNDC1 K119R-Flag). Tubulin served as loading control. **(E)** Alignment of partial FUNDC1 coding sequences from WT, FUNDC1 KO, and USP19/FUNDC1 DKO HeLa cells lines. **(F)** Western blot analysis of lysates from HEK293T cotransfected with the indicated plasmids. Tubulin served as loading control. **(G)** Western blot analysis of subcellular fractions from FUNDC1 KO-FUNDC1-Flag and FUNDC1 KO-FUNDC1 K119R-Flag cells exposed to hypoxia for 8 h. Cyto, cytosol; Mp, pure mitochondria; WCL, whole-cell lysate. **(H)** Quantification of the ratio of Flag-tagged FUNDC1 in the MAM in G. Bar represents mean ± SEM; unpaired two-tailed Student's *t* test, three independent experiments.

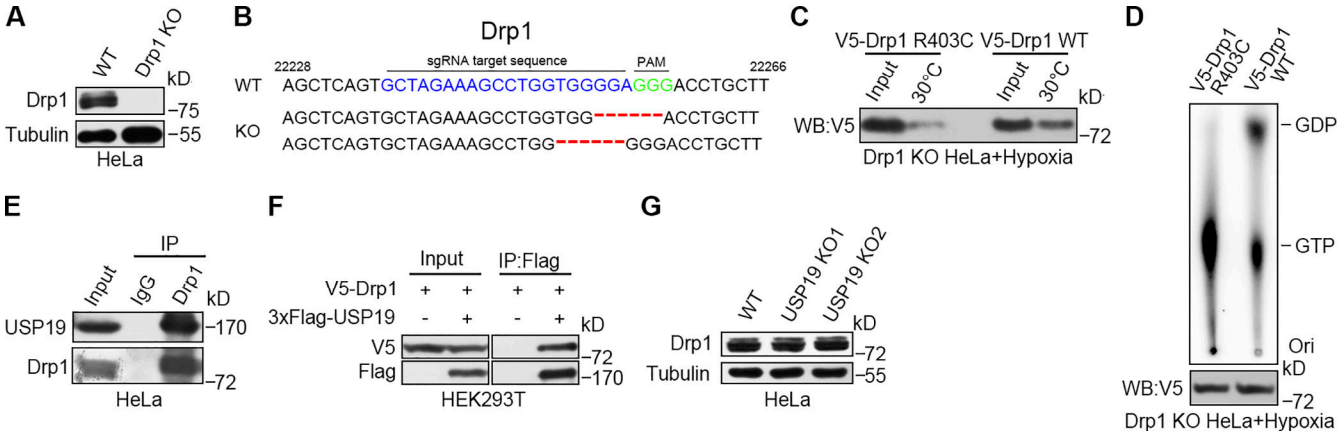

Figure S5. **USP19 interacts with Drp1, and the Drp1 R403C mutant impairs GTPase activity. (A)** Western blot analysis of lysates from WT and Drp1 KO HeLa cells. Tubulin served as loading control. **(B)** Alignment of partial Drp1 coding sequences from WT and Drp1 KO HeLa cell lines. Protospacer adjacent motif (PAM), green; sgRNA target, blue; mutated sequence, red. **(C)** Lysates from Drp1 KO HeLa cells expressing V5-Drp1 R403C or V5-Drp1 WT were exposed to hypoxia for 8 h and incubated with GTP-agarose beads. Samples were analyzed using Western blotting (WB) with an anti-V5 antibody. **(D)** Lysates from Drp1 KO HeLa cells expressing V5-Drp1 R403C or V5-Drp1 WT were exposed to hypoxia and immunoprecipitated with anti-V5 antibody. Immunopurified Drp1 was incubated with [α-32P] GTP and analyzed by TLC. Western blot analysis of V5-Drp1 served as loading control. **(E and F)** Lysates from HeLa cells (E) or HEK293T cells cotransfected with the indicated plasmids (F) were immunoprecipitated (IP) with anti-Drp1 (E) or anti-Flag (F) antibodies. Immunoprecipitated samples were analyzed using Western blotting. **(G)** Western blot analysis of lysates from WT and USP19 KO HeLa cells. Tubulin served as loading control.